Atmos. Chem. Phys. Discuss., 9, 6979–7032, 2009
www.atmos-chem-phys-discuss.net/9/6979/2009/

Atmospheric Chemistry and Physics Discussions

This discussion paper is/has been under review for the journal *Atmospheric Chemistry and Physics (ACP)*. Please refer to the corresponding final paper in *ACP* if available.

Ozone budget in the West African lower troposphere during the AMMA (African Monsoon Multidisciplinary Analysis) campaign

M. Saunois[1,2], C. E. Reeves[3], C. Mari[1,2], J. G. Murphy[3,4], D. J. Stewart[3], G. P. Mills[3], D. E. Oram[3], and R. M. Purvis[5,*]

[1]Université de Toulouse, UPS, LA (Laboratoire d'Aérologie), 14 avenue Edouard Belin, 31400 Toulouse, France
[2]CNRS, LA (Laboratoire d'Aérologie), 31400 Toulouse, France
[3]School of Environmental Sciences, University of East Anglia, Norwich, UK

[4]Department of Chemistry, University of Toronto, Toronto, Canada
[5]Facility for Airborne Atmospheric Measurement, National Centre for Atmospheric Science, Cranfield, UK
*now at: Facility for Ground Atmospheric Measurements, National Centre for Atmospheric Science, University of York, Heslington, York, UK

Received: 6 January 2009 – Accepted: 18 February 2009 – Published: 16 March 2009

Correspondence to: M. Saunois (marielle.saunois@aero.obs-mip.fr)

Published by Copernicus Publications on behalf of the European Geosciences Union.

Abstract

A bi-dimensional latitudinal-vertical meterological model coupled with O_3-NO_x-VOC chemistry is used to reproduce the distribution of ozone and precursors in the boundary layer over West Africa during the African Monsoon Multidisciplinary Analysis (AMMA) campaign as observed on board the Facility for Airborne Atmospheric Measurements (FAAM) BAe 146 Atmospheric Research Aircraft. The model reproduces the increase of ozone mixing ratios in the boundary layer observed between the forested region south of 13° N and the Sahelian area northward. Sensitivity and budget analysis reveals that the intertropical convergence zone is a moderate source of O_3 rich-air in the boundary layer due to convective downdrafts. Dry deposition drives the ozone minimum over the vegetated area. The combination of high NO_x emissions from soil north of 13° N and northward advection by the monsoon flux of VOC-enriched air masses contributes to the ozone maximum simulated at higher latitudes. Simulated OH exhibit a well marked latitudinal gradient with minimum concentrations over the vegetated region where the reactions with biogenic compounds predominate. The model underestimates the observed OH mixing ratios, however this model discrepancy has slight effect on ozone budget and does not alter the conclusions.

1 Introduction

One of the objectives of the African Monsoon Multidisciplinary Analyses (AMMA) project is to improve understanding of the ozone budget over West Africa. This paper adresses this for the lower troposphere by using a 2-D coupled chemistry dynamics model, the results of which are compared to concentration fields observed by a research aircraft.

Tropospheric ozone, O_3, is formed by photochemical oxidation of carbon monoxide, CO, and hydrocarbons in the presence of nitrogen oxides (NO_x). The formation of the hydroxyl radical, OH, by ozone photolysis is promoted in the tropics by high UV radia-

ACPD

9, 6979–7032, 2009

tion and temperature (Thompson, 1992). OH is the primary oxidant of the atmosphere and is responsible for the removal of many pollutants. In Africa primary pollutants come from biomass burning, natural emissions (vegetation, soils), lightning NO_x emissions and anthropogenic sources. These trace gases can have a significant impact on the atmospheric chemistry and lead to the formation of ozone.

African biomass burning results from agricultural practices and takes place during the dry season (Jonquière et al., 1998) contributing a large amount of the global emissions of CO, hydrocarbons and NO_x. During the monsoon (June, July and August) little biomass burning takes place over West Africa. However, biomass burning plumes from the Southern Hemisphere may be transported over the Atlantic Ocean to the Northern Hemisphere over West Africa (e.g., Jonquière et al., 1998; Sauvage et al., 2005, 2007b). Signatures of biomass burning plume intrusions have been observed during the AMMA campaign by radiosondings in Cotonou (Mari et al., 2008; Thouret et al., 2009) and airborne measurements on several research aircraft (Reeves et al., 2009).

Vegetation releases vast quantities of diverse volatile organic compounds (VOCs) (Kesselmeier and Staudt, 1999) and isoprene is one of the most important (e.g., Guenther et al., 1995). The effect of biogenic emissions from vegetation on ozone formation has been investigated in previous studies using global models by Wang and Eltahir (2000) and Pfister et al. (2008) showing an ozone change of up to 8 ppbv over West Africa. Using a global climate model, Aghedo et al. (2007) investigated the impact of biogenic trace gases (VOCs, CO and NO_x) emitted from Africa and showed that this source is the most important African emission source affecting the total tropospheric ozone.

As a catalyst for the ozone formation, NO_x influences the oxidative capacity of the atmosphere. Biogenic emissions of nitric oxide (NO) from soils remain uncertain and are highly controlled by surface soil temperature and moisture as well as nitrogen content in the soil. Evidence for large emission pulses of NO from West African Sahel soils wetted after a dry period were observed during AMMA (Stewart et al., 2008, and refer-

ACPD
9, 6979–7032, 2009

ences therein). Using satellite data Jaeglé et al. (2004) also showed that NO emitted from wetted soils can lead to a significant enhancement of NO_x concentrations over West Africa. Recent AMMA studies have linked the NO emission from wetted soils to ozone enhancement during the West African Monsoon (WAM) (July and August 2006) (Stewart et al., 2008; Delon et al., 2008).

The electrical activity associated with deep convection systems in the InterTropical Convergence Zone (ITCZ) (Christian et al., 2003) is a major source of NO in the upper tropical troposphere (Pickering et al., 1996; Bond et al., 2002; Labrador et al., 2005; Martin et al., 2007; Sauvage et al., 2007c) which has a large influence on the ozone distribution in the middle and upper troposphere (Martin et al., 2000; DeCaria et al., 2005, among others) due to its relatively long lifetime. Sauvage et al. (2007b) and Saunois et al. (2008) have studied the possible impact of lightning NO_x on the ozone meridional distribution in the upper troposphere over Africa. Deep convection causes entrainment of ozone precursors from the surface to the free troposphere (Lawrence et al., 2003) whilst downdrafts supply the planetary boundary layer (PBL) with O_3 rich air from aloft (Jacob and Wofsy, 1990). Consequently surface ozone might slightly increase due to lightning NO (Aghedo et al., 2007) and downdrafts of O_3-rich air.

In Africa anthropogenic emissions have a large spatial variability with highest impact from South Africa, Nigeria and Egypt. In the region of interest, West Africa, Nigeria is the country which likely contributes the most to anthropogenic emissions according to emission inventories. Anthropogenic release of trace gases has a strong local effect in highly populated cities (e.g., Lagos in Nigeria, Cotonou in Benin, Ouagadougou in Burkina) where urban pollution severly affects population health (Baumbach et al., 1995; Fanou et al., 2006; Linden et al., 2008). Using a global climate model (Aghedo et al., 2007) found an increase of surface ozone of about 2–7 ppbv in West Africa due to anthropogenic emissions during boreal summer with a maximum effect located in Nigeria.

The dry deposition of O_3 is one of the most important sinks for ozone in the boundary layer. The majority of O_3 flux experiments have been carried out during the dry season

ACPD
9, 6979–7032, 2009

(Kirchhoff et al., 1988; Gregory et al., 1988; Andrea et al., 1992; Cros et al., 1992, 2000; Matsuda et al., 2006; Rummel et al., 2007) in Congo and in Amazonia. The Amazonian Boundary Layer Experiment (ABLE) 2B (Fan et al., 1990), the experiment of Matsuda et al. (2006) in a tropical forest in Thailand and the LBA-EUSTACH experiment in Rondonia, Brazil (Rummel et al., 2007) reported continuous O_3 flux measurements above tropical forests during the wet season and calculated ozone dry deposition velocities in the range of 1.8–0.26 cm s^{-1}, 0.25–0.65 cm s^{-1} and 0.3–1.5 cm s^{-1} respectively depending on time of day. Using a one dimensional photochemical model for the planetary boundary layer, Jacob and Wofsy (1990) found that O_3 losses from deposition to the canopy reaches −2.0 ppbv day^{-1} leading to a net loss of O_3 in the PBL of the Amazon forest during the wet season.

During the AMMA campaign, ozone and trace gas measurements were made on board five aircraft (Reeves et al., 2009). Among them, the FAAM BAe-146 flew over West Africa from Niamey and sampled both the boundary layer and the free troposphere. The latitudinal variation of the land cover in West Africa (ocean/savanna/steppe/semi-desert/desert) leads to a latitudinal variation of biogenic emissions which can lead to horizontal gradients in trace gas concentrations in the lower atmosphere (Reeves et al., 2009; Murphy et al., 2009). In particular, the O_3 meridional profile in the boundary layer presents lower values over tree covered areas and higher values north to them where the soil is largely bare.

In this context, a 2-dimensional model is a useful numerical tool to investigate the relative importance of different chemical and physical processes influencing ozone and its precursors mixing ratios. Based on the zonal symmetry between 10° W and 10° E of (e.g.) vegetation cover, surface temperature and albedo, a 2-D model has been developed by Peyrillé et al. (2007) to simulate a typical July monsoon regime in a latitude-altitude cross section. This idealized model has already been used in a chemistry framework to study the impact of the lightning NO_x on the O_3 meridional profile in the upper troposphere (Saunois et al., 2008).

Section 2 presents a brief description of the measurements made to obtain the ob-

served data used in this study. Section 3 describes the 2-D idealized model along with the surface emissions and dry deposition velocities employed. Section 4 compares modelled and observed trace gases mixing ratios in altitude-latitude cross sections. The ozone budget in the layer 0–700 m is discussed in Sect. 5. Section 6 presents different sensitivity tests to investigate the influence of key factors (such as lightning, isoprene and terpene emissions, NO_x from wetted soils, ozone dry deposition and anthropogenic emissions) on the ozone distribution.

2 Experimental data

The measurements used in this study were made onboard the FAAM BAe-146 Atmospheric Research Aircraft which was based in Niamey, Niger for the AMMA campaign from 17 July to 17 August 2006. Flights were conducted in a region from 4° N to 18° N and 4° W to 6° E over West Africa, mainly over Benin and south-west of Niger, as well as regions of Mali, Burkina Faso and Togo (Reeves et al., 2009). The flights sampled both the boundary layer and the free troposphere. A summary of the measurements including measured parameters, precision and accuracies is listed in Table 1. NO_x was measured using a commercial TECO 42C chemiluminescence NO_x analyser, which measures NO from the chemiluminescence of reaction with ozone. NO_2 (and some other NO_y species) are converted to NO by a molybdenum converter. Ozone was measured using a TECO 49C UV photometric instrument. Carbon monoxide was measured by VUV resonance fluorescence using an Aero Laser AL5002 Fast Carbon Monoxide Monitor (Gerbig et al., 1999). Isoprene, acetone and the sum of methacrolein and methyl vinyl ketone were measured using a Proton Transfer Mass Spectrometer (PTrMS) supplied by Ionicon Analytik (Murphy et al., 2009). The technique is based on the transfer of a proton from H_3O^+ to organic compounds which have a higher proton affinity. The resulting ions are detected using mass spectrometry. The instrument produced a point (1–2 s) measurement for each species of interest approximately every 15 s. Formaldehyde was measured using a fluorescence technique based on the

ACPD
9, 6979–7032, 2009

Hantzsch reaction (Cardenas et al., 2000).

3 Model description

The idealized 2-D version of the Méso-NH model used for this study was initially designed by Peyrillé et al. (2007) to provide a latitudinal representation of the monsoon system and the associated circulation between 10° W and 10° E. Based on a similar 2-D approach Saunois et al. (2008) studied the budget of ozone in the upper troposphere. The model is based on the French community atmospheric simulation system Méso-NH (Lafore et al., 1998).

3.1 Model configuration

The 2-D model of Peyrillé et al. (2007) extends from 30° S to 40° N with a horizontal resolution of 70 km. The vertical domain extends to 20 km, with a stretched grid of 30 m near the surface to 1 km in the upper troposphere. A so-called sponge layer above 20 km is implemented as an upper boundary to prevent wave-reflection at the top. The lateral boundary conditions applied to the North and South of the domain allow tangential velocities but introduce zero forcing so that no interaction with the mid-latitudes is allowed. The West African subcontinent is approximated as a flat continental band between 5° N and 30° N. Orographically induced circulation is hence not considered. Peyrillé et al. (2007) have shown that adding a plateau induces a northward displacement of the monsoon of about 3°. The parameterization of convection is adopted from Bechtold et al. (2001), including transport and scavenging of soluble species (Mari et al., 2000). Turbulent processes are represented by the one-dimensional version of the turbulent scheme of Cuxart et al. (2000), based on the mixing length of Bougeault and Lacarrère (1989) and including a prognostical turbulent energy equation. Sea surface temperature (Atlantic Ocean and Mediterranean Sea) are taken from the Reynolds climatology of 1982–2003 (Reynolds and Smith, 1995) using July profiles for the Gulf

ACPD
9, 6979–7032, 2009

of Guinea and May profiles for the Mediterranean Sea. The role of the SSTs in the Mediterranean Sea has been discussed by Peyrillé et al. (2007). The flux parameterization over the ocean for tropical winds is implemented according to Mondon and Redelsperger (1998). The exchange between the surface and the atmosphere is described by the ISBA (Interactions between Soil, Biosphere and Atmosphere) scheme of Mahfouf and Noilhan (1996).

A reduced chemical scheme for tropospheric chemistry, ReLACS (Regional Lumped Atmospheric Chemical Scheme, Crassier et al., 2000), has been added to the dynamical model. This chemical scheme is a reduced version of the explicit chemical scheme RACM (Stockwell et al., 1997). This reduced mechanism was constructed following a "lumped molecule approach", in which the kinetic data and product yields for the mechanism (model) species (e.g. ALKA in Table 2) are calculated from the kinetic data and product yields of all real species (e.g. alkanes, alkyns, alcohols...) using emissions rates and reactivity as weighting factors. ReLACS considers 37 chemical species and 128 equations. Table 2 summarises the correspondence between some mechanism (model) species and the real species. Under this assumption, an emitted species can be represented by a model species which reacts at a different rate providing that an aggregation factor is applied to the compound emissions. These aggregation factors can be seen in the Table 3 where emissions fluxes are summarised. For example, for the model species ALKA, the emission of ALKA is equal to 0.44 times the emission of propane plus 0.85 times that of methanol.

A parameterization of the NO_x production by lightning (LNO_x) has been implemented into the deep convection scheme by Mari et al. (2006). The parametrization of the lightning frequency is based on Price and Rind (1992) and related to the convective cell height. The ratio IC/CG (IC stands for Intra-Cloud and CG for Cloud-to-Ground lightning) is derived from Price and Rind (1993) and depends on the depth of ice layers in the cloud. The NO production in the flashes is assumed to be proportional to air density along the flash. The specificity of this scheme is that it uses updraft and downdraft mass fluxes modeled by the deep convection scheme to generate the profile

ACPD
9, 6979–7032, 2009

of lightning NO_x. The LNO_x source is calibrated to 25 Mg(N)/month to obtain simulated ozone and NO_y mixing ratios in agreement with the measurements made on board the MOZAIC aircraft (Saunois et al., 2008).

The model is initialised with a quiet, horizontally homogeneous, and almost dry (10% relative humidity) atmosphere. For initialisation, the mixing ratios of the chemical species have been set to constant values (50 ppbv for O_3, 100 ppbv for CO, 10 pptv for NO and NO_2 and 1 pptv the others species), and the influence of the initial values is found negligible after 25 days of simulation. The model is then integrated for 30 days, with solar conditions corresponding to 15th July including diurnal variation.

3.2 Surface emissions

Table 3 summarises the set of surface emissions used in this study. To closely reproduce the observed distribution of ozone and its precursors, surface emissions follow the latitudinal land cover as observed during the period of measurements. As a consequence of the model configuration, ocean is considered south of 5° N and north of 30° N. Isoprene is known to be emitted from trees. Satellite data of leaf area index and visual observations from the research aircraft during AMMA showed tree cover to extend from the coast to 12–13° N. To the north was mostly bare soil. Consequently emissions from vegetation are considered between 5° N and 12° N in the idealized model and NO emission from soil between 5° N and 16° N, with low rates south of 12° N due to canopy reduction and higher values north of 12° N as there is little vegetation and many precipitation events at this time of the monsoon leading to NO pulses (Stewart et al., 2008; Delon et al., 2008). The values for the biogenic emissions fluxes have been derived from the POET/GEIA inventory (Granier et al., 2005) for the month of July except for isoprene and terpene. The isoprene emission flux is derived from the July 2006 estimation of Müller et al. (2008) based on MEGAN/MOHYCAN models and the terpene emissions are equal to those of isoprene scaled by 0.1. The emission fluxes have been averaged over the longitudinal band 5° W–5° E between −30° S and 5° N, 5° N and 12° N and 12° N and 16° N for ocean, vegetation and wetted bare soils areas

ACPD
9, 6979–7032, 2009

respectively. NO_x emission fluxes values have been adapted from both POET/GEIA inventory (Granier et al., 2005) and the work of Jaeglé et al. (2004). Except for emissions from vegetation, which have a diurnal variation with a maximum at 12:00 UTC, the emission fluxes are kept constant throughout the simulation. A set of anthropogenic emissions is included as well and is derived from the RETRO 2000 inventory (Schultz et al., 2005) and represents the averaged emissions flux between 5° W and 5° E in longitude. The latitudinal distribution of anthropogenic emissions shows higher values to the south due to higher population density near the coast. As a consequence, a two-step distribution is applied with higher (lower) values derived from the calculated mean between 5° N and 8° N (8° N and 14° N).

3.3 Dry deposition velocities

Table 4 summarises the dry deposition velocities used in this study. Velocities for dry deposition also follow the latitudinal land cover but do not have diurnal variations as expected in the real world. Deposition velocities for NO, NO_2, HNO_3, H_2O_2 were adopted from Seinfeld and Pandis (1998) and for HCHO, aldehydes, PAN from von Kuhlmann et al. (2003). The dry deposition velocity for ozone over ocean and desert is taken from Seinfeld and Pandis (1998). For ozone dry deposition over vegetation, the value of 0.65 $cm.s^{-1}$ is taken from Matsuda et al. (2006) who studied the ozone dry deposition over tropical forest in Thailand during the wet season. This value is in the range of the ones calculated by Rummel et al. (2007) from the LBA-EUSTACH 1 experiment during the wet season in Amazonia which range around 1.2 $cm.s^{-1}$ during daytime to 0.3 $cm.s^{-1}$ during nightime leading to a 24 h average velocity of 0.67 $cm.s^{-1}$ above canopy.

4 Meridional distribution of ozone and its precursors in the lower troposphere

A reference run is performed which include all the surface sources (biogenic and anthropogenic) as well as lightning emission of NO. Sensivity studies of ozone distribution to the emission is discussed in Sect. 6. Figure 1 to Fig. 6 shows the latitude-altitude cross sections of simulated and observed trace gases.

4.1 Hydrocarbons

BIO is the lumped species for isoprene and terpenes (Table 2) and its emissions correspond to 90% of isoprene and 10% of other terpenes (Table 3). Figure 1a, e shows the observed isoprene and simulated BIO cross sections. Similar to isoprene, BIO remains close to the vegetation sources due to its short lifetime. The typical lifetime of BIO at 12:00 UTC for its reaction with OH is 1.5 h in the lowest levels of the model and 30–45 min at 1 km reflecting the vertical gradient of OH south of 12° N (see Fig. 6). The BIO lifetime is also affected by its reaction with O_3 (1–1.5 days at 12:00 UTC). The longer lifetime of BIO near the surface favors a vertical mixing up to 1–2 km. At this altitude, BIO is rapidly oxidized as also found by Jacob and Wofsy (1990) in the Amazonian PBL during wet season. At 500 m, the simulated BIO mixing ratio (Fig. 1a) ranges between 0.7 and 1.0 ppbv in good agreement with the observed isoprene mixing ratios at the same altitude (Fig. 1e). CARBO is a lumped species for glyoxal and other carbonyls, including methacrolein (Table 2), and is essentially a product of the BIO oxidation. Its lifetime with respect to reaction with OH is longer than that of BIO (around 10 h near the surface and 2–3 h at 1 km) and allows it to be transported slightly further upwards and northwards (Fig. 1b). CARBO is initially produced within the lowest levels of the model but is rapidly oxidized above about 500 m and north of 12° N. Comparing the simulated concentrations of CARBO with the observations is not straightforward as, not only does CARBO represents many compounds, but the PTr-MS measurements of methacrolein (MACR) cannot be separated from that of methyl vinyl ketone (MVK), which is not represented by CARBO. Despite this the measured MVK+MACR

ACPD
9, 6979–7032, 2009

and simulated CARBO both show very similar distributions (Fig. 1b, f) which are slightly more widespread in altitude and latitude than the observed isoprene and simulated BIO (Fig. 1a, e). A quantitative comparison is unfortunately inappropriate between CARBO and MVK+MACR.

KET, lumped species for ketones, is treated chemically as 50% acetone and 50% MVK (Stockwell et al., 1997). Here again comparing measurements with model results is difficult. However the simulated KET distribution has the same pattern as the observed acetone both with maxima around 13–15° N (Fig.1c, g), which is quite different from that of the MVK+MACR. The simulated mixing ratios for KET are twice those observed for acetone (e.g. near the surface around 15° N KET is simulated to be up to 2.6 ppbv whereas observed acetone reaches only 1.3 ppbv). This is partly due to the lumped effect, but inaccuracies in emissions or the chemical scheme cannot be excluded.

The HCHO distribution is well simulated by the model with a northward extent up to 17° N and a vertical extent up to 2 km (with 0.6 ppbv at 2 km). Near the surface, the simulated HCHO mixing ratios range between 0.8 and 1.4 ppbv in reasonable agreement with the observed values (Fig. 1d, h). The model slightly overestimates HCHO near the surface.

4.2 Carbon monoxide

Both observed and simulated CO mixing ratios show higher values south of 13° N and lower to the north (Fig. 2). The model underestimates the CO mixing ratios compared to the BAe-146 measurements with only 120 ppbv at the maximum. This may be due to either underestimation of anthropogenic sources or natural emissions rates or assumptions in the chemical scheme. Jacob and Wofsy (1990) could not explained the CO enhancement in the Amazonian PBL by oxidation of biogenic hydrocarbons and showed that direct emissions from the forests account for 88% of the total modelled CO in the PBL. The multimodel comparison of Shindell et al. (2006) shows that underestimation of CO is a common behaviour of atmospheric chemistry models in particular

in the Northern Hemisphere extra-tropics. GEOS-Chem simulations of the tropical troposphere underestimate CO in the African lower troposphere (Sauvage et al., 2007a). These results suggest an underestimate of CO emissions, although a deficiency in the chemical scheme cannot be excluded. However sensitivity tests detailed later in Sect. 6 show that isoprene oxidation accounts for around 10% of the total modelled CO below 700 m. Artificially increasing OH concentration to avoid too much OH depletion over tree does not improve the CO comparison. Consequently these latter results suggests an underestimation of direct CO emission from vegetation. It is worth noting that the CO maxima values observed in the free troposphere above 2 km and south of 8° N are the consequence of biomass burning intrusions from the Southern Hemisphere (Mari et al., 2008; Reeves et al., 2009; Murphy et al., 2009). This additional source however is out of the bounds of the model. Enhancements in HCHO, NO_x and O_3 (Fig. 1b, 3b, 4b) at this altitude and latitude are signatures of this biomass burning intrusion as well. The simulated budget of CO in the lower troposphere shows a loss of CO by convective transport of CO-rich air out of the PBL. Photochemical production and loss of CO in the PBL is dependant on the altitude and latitude. Net photochemical production of CO takes place below 1–1.5 km and between 5° N and 13° N while net photochemical destruction of CO occurs elsewhere in the domain (not shown).

4.3 Nitrogen oxides

Figure 3 shows the observed and simulated NO_x meridional distribution. The simulated NO_x mixing ratios are clearly controlled by the meridional gradient of the emission rates. The highest values of NO_x are found north of 12° N where emission rates from bare soils have been assumed to be higher with up to 1 ppbv near the surface. At 500 m altitude simulated NO_x reached 500 ppt between 13° N and 17° N in good agreement with the observations. A secondary maximum near the surface is found around 7° N due to anthropogenic emissions. The observed surface NO_x mixing ratios show high values around urban area (6.5° N for Cotonou and 13° N for Niamey). This local effect is smoothed by the model due to the idealized variation of emissions and the coarse

ACPD
9, 6979–7032, 2009

resolution used (70 km). The high values of NO_x observed south of 6° N at 2–5 km (Fig. 3b) are a signature of the biomass burning plume intrusion from the Southern Hemisphere.

4.4 Ozone

Figure 4 presents the observed and simulated ozone distributions. The observed distribution of O_3 is characterized by a vertical gradient with lower values in the boundary layer and a strong meridional gradient at 14° N below 2 km. These patterns are well reproduced by the model. Lower values of O_3 below 2 km and south of 13° N are well captured by the model and range between 20 and 30 ppbv in reasonable agreement with the observations. These lower values south of 13° N are partly due to rapid deposition to trees as discussed by Reeves et al. (2009) and summarized by Janicot et al. (2008). Mixing ratios higher than 40 ppbv are obtained in the boundary layer around 15–16° N in both the model and observations. In the middle troposphere, the high O_3 values observed at 2–5 km at 6–8° N correspond to the biomass burning plume previously mentioned. The simulated budget of O_3 in the PBL is regulated by three main processes: a downward transport from the free tropopshere, deposition to the surface (especially over vegetation) and photochemistry. The ozone convective tendency in the PBL is positive (Fig. 5) showing that convection acts as a source of ozone through downward transport from the free troposphere. Photochemical production and loss of O_3 in the PBL is strongly dependant on altitude, latitude and time. During daytime, net photochemical destruction of O_3 takes place above 1200 m while net photochemical production (Fig. 5) occurs in the lowest levels of the model where the NO concentration is higher (Fig. 3). A comparison of the reaction rates of the peroxy radicals with HO_2 or NO at 12:00 UTC shows that the peroxy radicals preferentially react with HO_2 above 700 m while their reaction with NO is favoured below 1 km in higher NO conditions leading to the formation of NO_2 and then O_3. The threshold NO concentration for net photochemical O_3 production in the model is function of the latitude: 60 ppt of NO_x and 15 ppt of NO over vegetation, 100 ppt of NO_x and 30 ppt of NO north of 12° N.

ACPD
9, 6979–7032, 2009

These different thresholds seem to be linked to the amount of VOC available. Jacob and Wofsy (1990) found a crossover NO concentration of about 5 ppt over Amazonia during the wet season. The different VOC amount available in the two experiments might explained the different thresholds. The O_3 production rate is a function of NO_x mixing ratios and reaches more than 0.6 (1.2) ppbv h^{-1} south (north) of 12° N. Jacob and Wofsy (1990) also simulated a production rate of O_3 of up to 0.5 ppbv h^{-1} in lower NO_x conditions. Below that level, O_3 is photochemically destroyed.

4.5 Hydroxyl radical OH and HO_2

Figure 6 shows the modelled OH and HO_2 distributions at a given day at 12:00 UTC. A sharp gradient of OH is simulated around 13° N, with much lower concentrations to the south due largely to rapid loss by reaction with BIO over vegetation in the model. The simulated OH distribution is related to the O_3 in the PBL but the gradient of OH is sharper than the O_3 gradient. The modelled HO_2 distribution presents a similar pattern with higher values to the north (6–8×10^8 molecules cm^3 s^{-1}). Unfortunatly HO_x measurements performed on board the BAe during AMMA are too sparse geographically and temporally to show any latitudinal variation that could be compared with the model results. However some model to observation comparisons suggest that the model might underestimate OH and overestimate HO_2 (not shown). The low OH calculated by the model in the region of high isoprene concentration is typical of many models as discussed by Lelieveld et al. (2008). Here we address the influence of a possible misrepresentation of HO_x on the ozone and its precursors concentrations. This has been assessed through an artificial OH recycling as suggested by Butler et al. (2008) within the reaction between isoprene peroxy radicals BIOP and HO_2 that leads to isoprene peroxides. Including this recycling increases the OH concentration over vegetation by a factor of 2–3, but this reduces the agreement with the observed concentrations of isoprene (Fig. 7c). This direct effect could be improved by reducing the reaction rate between OH and isoprene to take account of the artificial mixing of short-lived species

ACPD
9, 6979–7032, 2009

in models of this grid size (Krol et al., 2000). However this substantial change in HO_x and isoprene induced only a small change in the PBL isoprene products (CARBO, KET and HCHO) and overall it led to insignificant change on the ozone latitudinal distribution (Fig. 7a). These results suggest that the misrepresentation of HO_x, if there is any, will not alter the following discussion about the ozone budget in the PBL.

5 Trace gas chemistry in the West African boundary layer (below 700 m)

The flights dedicated to the boundary layer survey were below 700 m and mostly between 300 and 600 m a.s.l. The layer 0–700 m is mostly within the observed BL (Stewart et al., 2008) which is in agreement with the boundary layer height simulated by the model and diagnosed with the turbulent kinetic energy (0.7–2 km). In the following we focus the study on the layer below 700 m where most of the data were collected and where the surface effects and the trace gas gradients are well pronounced.

5.1 Trace gas meridional profiles below 700 m

Figure 7 compares the modelled meridional profiles of trace gases with the measurements. Measurements have been averaged in latitude to the horizontal grid of the model and in altitude from the surface up to 700 m. The observed profiles (box plots) as well as the simulated profiles (solid or dashed lines) are presented in Fig. 7. The reference run is the black solid line and the other lines correspond to sensitivity tests discussed later in the paper.

As shown in Fig. 7c, the isoprene mixing ratios are captured well by the model species BIO between 7 and 11° N with values close to the median of the observations or inside the interquartile range. Discrepancies appear to both sides of this area where the model overestimates the isoprene mixing ratios possibly due to emissions from vegetation assumed in too a large latitudinal band. The coast in the model is set at 5° N while the coast is located at 6° N near Cotonou where the aircraft flew explain-

ing the model observation differences around 5–6° N. Also the MEGAN/MOHYCAN emissions shows a general agreement with the observed isoprene. However the observations suggest that emissions drop off toward the coast and 12° N whereas the model emissions are constant between 5 and 12° N. The same discrepancy is found for HCHO, CO and CARBO (compared to MVK+MACR) (Fig. 7d,e,f). The CO mixing ratio is largely underestimated south of 13° N as discussed previously. At 7° N and 13.5° N, the measured CO, HCHO and NO_x concentrations are higher and correspond to pollution from the cities of Lagos (Hopkins et al., 2009) and Niamey, respectively. CARBO and MVK+MACR do not compare well quantitatively, as discussed previously, but their meridional variations are reasonably similar given the latitudinal shift of the drop-offs resulting from the modelled BIO distribution described above. The acetone profile exhibits a much broader maximum than does KET.

The modelled NO_x agrees reasonably well with the measurements in that they are mostly within the interquartile range. It is, however, hard to discern a clear latitudinal gradient in the observations, partly because the data at 7° N and 13.5° N are skewed by pollution from the cities of Lagos and Niamey and partly because the data exhibit considerable variability due to largely instrumental noise and to some extent atmospheric variability. The TECO NO_x has a detection limit of 50 ppt with a 2 min averaging time while the data is reported as 10 s data leading to a detection limit of at least a few hundred ppt. By averaging over grid boxes we are considering enough data such that the median should be reasonably robust value and give some indication of how NO_x varies with latitude. Another point is that the TECO NO_x measurements includes a fraction of NO_z (Stewart et al., 2008). Comparing two instruments NO_{xy} and TECO during AMMA it looks like on average TECO NO_x was about 16% higher than NO_{xy} NO_x. Unfortunately the NO_{xy} instrument was not operational on many flights so the data are too sparse to provide a good representation of the latitudinal gradient of NO_x and hence why the data from the TECO have been used. Given the uncertainty in the measurements, the model NO_x are in the range of observations. The simulated NO_x profile does not reproduced the spatial variability of the measurements due to the

ACPD
9, 6979–7032, 2009

idealized emissions and exhibits too sharp a gradient between 12° N and 16° N. NO_x mixing ratios seem slightly overestimated by the model.

As shown in Fig. 7a, the O_3 model to measurement comparison is rather good though it shows also a few discrepancies linked to points already mentioned for the VOCs and the NO_x. The O_3 values simulated in the reference run (black line) between 7 and 13° N are in reasonable agreement with measurements. The model fails to reproduce the higher values of O_3 further south probably due to an overestimated sink of O_3 from dry deposition because of the misplaced coast. The model simulates the O_3 maximum 1° further north. This shift seems to be linked to the discrepancies for the VOCs and NO_x. The VOCs being further north permit O_3 formation further north too. The model resolution is probably too coarse to expect a perfect agreement for the ozone maximum location which can be shifted by ±1° in latitude depending on the vegetation extent in the model. Also the simulated meridional gradient is not as sharp as the observed one.

Despite some discrepancies, the reasons for many of which are known and understood, the idealized 2-D model reproduces well the main trace gases variations. In the next two subsections, the northward advection associated with trace gases transport during the night and the O_3 budget in the PBL are discussed.

5.2 Northward advection by the monsoon flux

The ozone maximum in the BL is found further north of the vegetation where the more reactive VOCs (isoprene, MVK and MACR) are lower and not directly emitted. This suggests that either hydrocarbons are transported to the north where higher NO_x mixing ratios are found leading to enhanced ozone production or ozone is produced over the source region is then transported to the north or both. Both assumptions need a northward advection of materials. During nighttime the south-easterly monsoon flux becomes stronger (Parker et al., 2005; Peyrillé and Lafore, 2007) while OH, the main oxidant, concentrations decrease leading to longer lifetimes of the pollutants such as isoprene and its oxidation products. These two mechanisms favour a northward advection of materials in the boundary layer during the night. During the AMMA campaign on

25 July 2006, an afternoon flight (B219A) which presented peak biogenic emissions, has been followed by an later flight (B219B) after dark to study how the chemical composition has evolved and the nocturnal winds have redistributed the air. During the night flight, biogenic species were observed transiently, north to the wooden region, suggesting nocturnal advection with a northward wind of around 4 m s^{-1} (Murphy et al., 2009). This rough estimate is in agreement with the simulated zonal wind in the model below 1 km. The northward advection is clearly seen in the simulation when looking at the CARBO diurnal cycle below 700 m (Fig. 8). CARBO is advected northward during the night where the simulated meridional wind is up to 6 m s^{-1} allowing these species to be transported by more than 1° in 5 h 30 min whilst being still produced during nighttime via OH, O_3 and probably NO_3 oxidation. Consequently the northward advection by the monsoon flux appears to be a key process to transport VOCs to NO_x-richer region and certainly has an influence on the ozone distribution has discussed below.

5.3 Ozone budget below 700 m

Figure 9 presents the 24 h average of the ozone tendencies in the layer 0–700 m between 4° N and 19° N, plotted along with the meridional ozone concentration profile which exhibits the strong gradient at 13° N. As mentioned previously convection acts as a source of ozone by bringing ozone-rich air from the free troposphere to the boundary layer within the downdrafts with a maximum effect at 10–12° N. Convection is not the main driver leading to the modelled ozone gradient since on average the impact of convection on the layer 0–700 m is higher south of 12° N (Table 5) in contrast to that required to produced the observed ozone concentration pattern.

The turbulent tendency sign gives information on the net budget for emitted chemical species at the surface (=emission rate – deposition rate) combined with vertical mixing effect. For ozone the turbulent tendency is negative revealing a strong effect of dry deposition especially over vegetation where a higher deposition velocity is assumed (Table 4). Deposition contributes to a loss of O_3 (removing 0.40 ppbv/h over vegetation during daytime) balancing the ozone net chemical production and leading to lower O_3

ACPD
9, 6979–7032, 2009

mixing ratios south of 12° N .

The negative ozone chemical tendency over ocean shows that simulated ozone is destroyed over ocean where NO_x concentrations are low as found by Stickler et al. (2007) over the Atlantic Ocean near the Guyanas. North of 5° N, the net ozone chemical production is positive with values in the range of 0.2–0.7 ppbv/h depending on the latitude. Higher O_3 chemical production (Fig. 9) is collocated with higher NO_x mixing ratios (Fig. 7b) suggesting a NO_x-limited regime for ozone. The higher O_3 production rate to the north is twice the O_3 production over vegetation (Table 5) and contributes to creating the ozone maximum.

It is worth noting that the maxima in ozone mixing ratios and ozone chemical tendency are 1° apart (Fig. 9). This difference might be explained by the northward advection of materials by the monsoon flux as discussed previously. The positive (negative) horizontal advection of O_3 to the north (south) supports this explanation (Table 5).

The study of the mean meridional profiles suggests that both greater deposition over trees and higher ozone production to the north contribute to creating the ozone gradient by decreasing concentrations to the south and increasing them to the north respectively. Questions remain regarding firstly the relative contributions of the precursors involved in the ozone production (to the north and south of 13° N) and secondly the relative contributions of deposition and chemical production.

The contribution of species to the OH reactivity defined as the OH rate constant for a specific species mulitiplied by its concentration has been evaluated for the simulated results taken on 26th day at 12:00 UTC and averaged for the layer 0–700 m. The results of this calculation are shown in Fig. 10, including only model species that contribute more than 0.1% of the total. Methane is not calculated and is set at a constant value of 1800 ppbv but the peroxy radical formed from its reaction with OH is simulated and is called MO2 (methyl peroxy radical). As Fig. 10 shows, BIO contributes most to the OH reactivity over vegetation at 61% of the total at 10° N. The next most important species are CO and HCHO that contribute to 9% and 6% respectively as well as high peroxides OP2 (6%) which yields mainly ALKAP radicals. These results are similar to those of

Sumner et al. (2001) for the PROPHET 1998 summer experiment above a forested site in northern Michigan, which reported contributions of 75%, 10% and 4% for isoprene, formaldehyde and CO respectively. The contributions change to the north where BIO contributes to less than 0.1% of the total. At 16° N, CO, methane and HCHO contribute most to OH reactivity with 40%, 20% and 17% of the total. The next most important are peroxides OP1 and OP2 with 6% each (yielding MO2 and ALKAP peroxy radicals mainly) and then ALD and KET with 3% each both forming CARBOP peroxy radicals. These reactions with OH lead to the formation of peroxy radicals. Below 700 m, in relatively high NO conditions, the reactions of the peroxy radicals with NO dominate over those with HO_2. These reactions with NO yield NO_2 promoting photochemical production of O_3. To assess which peroxy radicals are most involved in the O_3 production, the loss rates of NO due to its reaction with five peroxy radicals are analyzed for 12:00 UTC when these radical concentrations maximize. The five peroxy radicals considered are: BIOP (peroxy radicals formed from BIO), CARBOP (acetyl peroxy radicals and peroxy radicals formed from KET, CARBO and ALD), ALKAP (peroxy radical formed from ALKA and OP2), ALKEP (peroxy radical formed from ALKE) and MO2 (methyl peroxy radical formed from CH_4 and OP1). The NO loss rates for these reactions are defined as the NO reaction rate constant for a specific radical multiplied by the radical and NO concentrations. Figure 11 presents the mean NO loss rates for the layer 0–700 m for its reaction with these five radicals as evaluated at 12:00 UTC on the 26th day. South of 14° N, the reaction of NO with BIOP is dominant as expected with up to 0.3 ppt s^{-1}. The four others contribute less than 0.05 ppt s^{-1} south of 12° N. At 14° N BIOP does not contribute much while ALKAP and MO2 lead to 0.13 ppt s^{-1} each and ALKEP and CARBOP to half of that. At 16° N, where O_3 production is at a maximum, MO2 contributes 0.15 ppt s^{-1}, ALKAP to half of that and CARBOP a third. Over vegetation ozone production is mostly the result of BIO oxidation whereas to the north CO, HCHO, methane, peroxides and ALKA contribute most to ozone production.

ACPD
9, 6979–7032, 2009

6 Influences of key factors on the ozone distribution and gradient below 700 m

This section investigates the influence of key factors (such as lightning, isoprene and terpene emissions, NO_x from soils, ozone dry deposition and anthropogenic emissions) on the ozone distribution through sensitivity studies (Sects. 6.1 to 6.5).

6.1 Influence of lightning

Lightning production of NO has been calibrated in Saunois et al. (2008). Including NO from lightning has no significant influence on NO_x mixing ratio in the boundary layer as production only takes place in the updrafts of the convection scheme. However an ozone increase in the UT due to LNO_x leads to an O_3 increase in the LT via the transport of ozone by the downdrafts in the convective systems (Fig. 9). Thus including LNO_x increases the ozone mixing ratio by ~2 ppbv in the boundary layer (not shown). However this increase is uniform in latitude and does not contribute to creating the observed ozone gradient. The slight increase of ozone when including lightning NO_x production leads to higher OH concentrations, but changes in BIO or CO through oxidation are not significant (50 ppt and 2–3 ppbv, i.e. 3% and 1.5% respectively).

6.2 Influence of anthropogenic emissions (run NOANT)

The results from the NOANT run are represented with the red line in Fig. 7. As explained in the model description section, the BAe-146 flew mostly over low population density areas except near Niamey and the Guinea Coast. The averaged RETRO emissions between 5° W and 5° E showed that most pollutants are emitted near the Guinea Coast thus higher emission rates were considered between 5° N and 8° N than between 8° N and 14° N. Greater changes in CO and especially in NO_x below 12° N are simulated (Fig. 7b, e). Including anthropogenic emissions increases CO mixing ratios by 30–35% which leads to better representation of the observed CO concentration but still lower than observed as discussed in Sect. 4.2. NO_x mixing ratios change essen-

ACPD
9, 6979–7032, 2009

tially south of 14° N with values higher by up to 50%. The influence on ozone is mostly seen in the south (up to 10%) with only a slight increase of 3% simulated at 17° N. This corresponds to an increase of 1–3 ppbv similar to the range of the impact of anthropogenic emissions on surface ozone as simulated by the global model ECHAM5-MOZ in Aghedo et al. (2007) (2–5 ppbv over West Africa for the boreal summer season, Nigeria excluded). Adding anthropogenic emissions leads to a change in the atmosphere oxidation capacity over West Africa and BIO, CARBO, HCHO and KET decrease by 20%, 15%, 17–20%, 10–13% respectively (Fig. 7c, d, f, g). The shape of the meridional profile of surface ozone over vegetation is significantly modified by anthropogenic emissions: the lower values are not as well-marked as the observations and the gradient ocean/land is not well reproduced when including anthropogenic emissions. The idealized two step distribution considered for anthropogenic emissions does not allow the model to reproduce well the local pollution sampled over Cotonou (6–7° N) and Niamey (12–13° N) where higher emissions and mixing ratios may be calculated at a smaller spatial scale. However these results indicate no significant contribution of anthropogenic emissions to the establishment of the ozone gradient at 14° N.

6.3 Influence of isoprene and terpenes (run NOISO)

Sensitivity studies have been performed to investigate the role of isoprene and terpenes on the ozone chemistry in the BL. Turning off the BIO species emissions in the model affects both the amount of VOCs in the troposphere and the oxidative capacity of the atmosphere. Due to non-linear effects, it is therefore difficult to estimate the contribution of isoprene to tropospheric chemistry. Pfister et al. (2008) have used a tagging chemical scheme to quantify the impact of isoprene on species containing carbon (such as CO and HCHO) and also to assess the impact of non-linearity. However, the use of a tagging scheme is limited and can not resolve species such as OH, O_3 or NO_x. To discuss the impact on ozone in this study we use a run called NOISO in which the model BIO source is switched off (green line Fig. 7). It is worth noting that other biogenic hydrocarbons such as alkanes, acetone or alcohols are also directly emitted

ACPD
9, 6979–7032, 2009

by vegetation (see Table 3).

When isoprene and terpene emissions are switched off, the CARBO species is clearly not produced by the chemical scheme, since it mainly results from the BIO oxidation. KET, HCHO and CO mixing ratios are decreased by 60–75%, 40–45%, 10–15% respectively when excluding isoprene and terpene. Granier et al. (2000) using a colouring technique (similar to the tagging of Pfister et al., 2008) have found that isoprene (terpenes) contribute to 15–20 (3–4) ppbv of surface CO over West Africa. In the Pfister et al. (2008) tagging study the contribution of isoprene to the surface is similar to the contribution to the CO (HCHO) column and range around 13–15% (40–50%) in West Africa. The non-linearity effect would lead to slightly larger (smaller) changes in CO (HCHO) as shown by Pfister et al. (2008). Considering that different isoprene inventories can change CO surface mixing ratios by about ±20% (Pfister et al., 2008) our results are in the range of the previous study values.

Ozone is less influenced by the BIO chemistry over vegetation than it is north of the forested area where O_3 changes by up to 5 ppbv. These results are in the range of the surface ozone mixing ratio increases found by Wang and Eltahir (2000) over West Africa (up to 8 ppbv) when isoprene emissions were included in a chemistry transport model (CTM). Small changes in ozone on a global scale are simulated by Pfister et al. (2008), though regional differences in surface ozone are large (up to 5 ppbv) and the largest absolute increase of column ozone is simulated over Equatorial Africa. These 2-D model results suggest a NO_x-limited ozone regime, indeed the ozone chemical tendency slightly increases when including isoprene.

Including BIO emissions leads to a slight decrease of NO_x mixing ratio mainly explained by PAN formation. The mean daytime simulated values for PAN range from 0.01–0.05 ppt without and 0.1–0.3 ppt with BIO emissions in agreement with the global study of Wang and Eltahir (2000). Despite the importance of the thermal decomposition of PAN at 300 K that leads to an approximate lifetime of 30 min for PAN, the high quantity of carbonyl radicals (called CARBOP in ReLACs) in the middle of the day balance the low values of NO_x and leads to PAN formation as reported in previous

studies (Singh et al., 1990; Jacob and Wofsy, 1990 during the wet season experiment in Amazonia ABLE2B and Doskey et al., 2004 over grassland in Illinois). Conversion of NO_x to PAN over vegetation and northward transport by the monsoon flux leads to decreased NO_x concentrations over trees while increasing them north of 14° N. As the ozone regime is NO_x-limited, including BIO may thus decrease the ozone chemical production over vegetation and increase it to the north. This impact of BIO on NO_x combined with possible ozonolysis of BIO and its products can explain the slight decrease of O_3 simulated over vegetation. As for the lower O_3 maximum simulated at 16° N, the ozone chemical production is sensitive to the amount of VOCs available in spite of the NO_x-limited regime for ozone.

6.4 Influence of NO_x from wetted soils to the north (run IDSOL)

In the reference run, higher NO_x emissions from soils are assumed north of 13° N as a consequence of the response of bare soils to precipitation. In the IDSOIL run (Fig. 7, blue line), the NO_x emission fluxes are equal north and south of 13° N leading to NO_x mixing ratios of around 200–250 ppt near the surface. A maximum of NO_x is simulated north of 13° N probably due to the monsoon flux transport and conversion from the PAN reservoir. Changing this NO_x source changes the O_3 distribution in the middle troposphere and near the surface south of 12° N by very little (less than 1 ppbv for the mean daytime values). In contrast, the O_3 mixing ratio decreases by up to 7 ppbv near the O_3 maximum at the surface near 16° N. An ozone gradient of about 10 ppbv is still simulated. However the ozone gradient in the reference run is sharper than in the IDSOIL run. There is almost no change in the distribution of the hydrocarbons: 2–4% more and lower NO_x emissions due to a slight decrease in OH and of the oxidising capacity of the atmosphere. The NO_x emission fluxes considered in the model which are adapted from POET /GEIA inventory and Jaeglé et al. (2005) (2×10^{10} and 4.5×10^{10} molecules $cm^{-2}\,s^{-1}$) are in the range of the calculated flux by Stewart et al. (2008) (5.1–11.2 ng N $m^{-2}\,s^{-1}$ i.e. 2.2–4.8$\times10^{10}$ molecules $cm^{-2}\,s^{-1}$) and Delon et al. (2008) (2–35 ng N $m^{-2}\,s^{-1}$ i.e. 1–15$\times10^{10}$ molecules $cm^{-2}\,s^{-1}$). Varying the

ACPD
9, 6979–7032, 2009

NO_x flux in the 2-D model would change the ozone level, however, the chosen values seem to be appropriate to reproduce the average ozone and NO_x observed levels below 700 m. Assuming higher emissions of NO_x from the bare soils allows higher values of O_3 mixing ratio in better agreement with observations. Higher NO_x from bare soils are not necessary to create the ozone meridional gradient but certainly do contribute to it with a higher maximum in the north.

6.5 Influence of ozone dry deposition over trees (run NODEP)

Ozone deposition is the major sink for ozone over vegetation. The sensitivity test called NODEP was performed to assess the contribution of dry deposition to the lower ozone mixing ratios simulated between 5° N and 13° N in agreement with the observations. O_3 dry deposition is omitted in the whole domain in the NODEP run.

O_3 dry deposition leads to a loss of about 3–4, 5–10 and 5 ppbv of surface O_3 over ocean, vegetation and bare soils/desert, respectively (Fig. 7 grey dashed line). The largest influence is seen over vegetation where the dry deposition velocity of ozone was assumed to be higher. Deposition decreases the oxidation capacity of the atmosphere by lowering the O_3 and subsequently OH levels, so that CO and BIO are oxidized less (2–3 ppbv and 300 ppt, respectively). Including O_3 deposition allows the low ozone concentrations observed over vegetation and a significant gradient to the north to be simulated.

Considering the three runs (RETRO, NODEP and IDSOL), the results show that the lower values of ozone over vegetation are essentially controlled by dry deposition over trees and that the ozone maximum is clearly a consequence of higher NO_x mixing ratios north of 13° N combined with northward advection of ozone and nitrogen species as well as hydrocarbons. The amount of VOCs emitted by the vegetation, especially in isoprene and terpenes, also contributes to the ozone maximum with a contribution of two thirds of that due to higher soil NO emissions. The other sources (lightning and anthropogenic) modify the ozone levels to some extent but do not contribute to the ozone gradient.

7 Conclusions

Well marked meridional gradients in trace gas concentrations have been observed during the wet season in the lower troposphere of West Africa during the AMMA 2006 campaign. These horizontal variations are related to the latitudinal variations of the land cover in West Africa which leads to emission and deposition changes with latitude. A two dimensional model (latitude vs altitude) has been used to determine which processes are involved in creating these gradients. Idealized latitudinal distributions for emission fluxes have been adapted from various emission inventories to account for both natural and anthropogenic emissions.

The model reproduces the observed lower troposphere latitudinal variation in ozone extremely well along with the spatial distribution and magnitude of biogenic compounds and nitrogen oxides. Higher concentrations of isoprene and CO are found near the vegetated area (5° N–12° N). High values of NO_x are simulated around 15° N as a response to the assumption of higher soil NO emissions between 12° N and 16° N resulting from pulses over recently wetted soils (Stewart et al., 2008; Delon et al., 2008). The O_3 vertical and meridional gradient is well reproduced. Model diagnostics are used to study the ozone budget in the layer 0–700 m in which ozone is minimum over vegetation and maximum around 15–16° N. Simulated trace gas variations in this layer are compared well with the observations despite discrepancies to the south due to the different position of the coast in the model compared with the real coast location in the studied AMMA area.

The model diagnostics show that convection bringing O_3-rich air from the free troposphere to the BL due to downdrafts is not a driver leading to the ozone gradient. Sensitivity tests exclude clear contributions of lightning or anthropogenic emissions in creating this gradient. Ozone dry deposition has a strong effect over vegetation and controls the ozone minimum. Since the ozone chemical regime is NO_x limited, ozone production is promoted to the north over bare soils where soils NO emission is assumed higher. The northward advection by the monsoon flux of materials, especially

ACPD
9, 6979–7032, 2009

secondary or longer lived hydrocarbons to a NO_x-rich region contribute substantially to the ozone maximum. Short-lived species such as isoprene contribute most to the OH reactivity over trees while longer-lived and secondary product hydrocarbons are oxidized north to the forested area where they are transported and/or produced and contribute to the ozone maximum. Further study is now required on the isoprene chemistry over West African forests and savannas to confirm this scenario (Murphy et al., 2009).

Acknowledgements. Based on an French initiative, AMMA was built by an international scientific group and is currently funded by a large number of agencies, especially from France, the United Kingdom, the United States, and Africa. It has been the beneficiary of a major financial contribution from the European Communities Sixth Framework Research Programme. Detailed information on scientific coordination and funding is available on the AMMA International Web site at www.amma-international.org. Computer time has been provided by the Institut du Développement et des Ressources en Informatique Scientifique (IDRIS). This work was partly funded by the UK Natural Environment Research Council through tha AMMA-UK Consortium grant and received support from the National Centre for Atmospheric Science (NCAS), including Facility for Airborne Atmospheric Measurements and the British Atmospheric Data Centre.

The publication of this article is financed by CNRS-INSU.

References

Aghedo, A. M., Schultz, M. G., and Rast, S.: The influence of African air pollution on regional and global tropospheric ozone, Atmos. Chem. Phys., 7, 1193–1212, 2007, http://www.atmos-chem-phys.net/7/1193/2007/. 6982, 6983, 7002

Andrea, M., Chapuis, A., Cros, B., Fontan, J., Helas, G., Justice, C., Kaufman, Y., Minga, A., and Nganga, D.: Ozone and Aitken nuclei over Equatorial Africa: Airborne observations during DECAFE 88, J. Geophys. Res., 97, 6137–6148, 1992. 6984

Baumbach, G., Vogt, U., Hein, K., Oluwole, A., Ogunsola, O., Olaniyi, H., and Akeredolu, F.: Air pollution in a large tropical city with a high traffic density – results of measurements in Lagos, Nigeria, Sci. Total Environ., 169, 25–31, doi:10.1016/0048-9697(95)04629-F, 1995. 6983

Bechtold, P., Bazile, E., Guichard, F., Mascart, P., and Richard, E.: A mass-flux convection scheme for regional and global models, Q. J. Roy. Meteor. Soc., 127, 869–886, 2001. 6986

Bond, D. W., Steiger, S., Zhang, R., Tie, X., and Orville, R.: The importance of NO_x production by lightning in the tropics, Atmos. Environ., 36, 2002. 6983

Bougeault, P. and Lacarrère, P.: Parametrization of orography induced turbulence in a mesobeta-scale model, Mon. Weather Rev., 117, 1872–1890, 1989. 6986

Butler, T. M., Taraborrelli, D., Brühl, C., Fischer, H., Harder, H., Martinez, M., Williams, J., Lawrence, M. G., and Lelieveld, J.: Improved simulation of isoprene oxidation chemistry with the ECHAM5/MESSy chemistry-climate model: lessons from the GABRIEL airborne field campaign, Atmos. Chem. Phys., 8, 4529–4546, 2008, http://www.atmos-chem-phys.net/8/4529/2008/. 6994

Cardenas, L. M., Brassington, D. J., Allan, B. J., Coe, H., Alicke, B., Platt, U., Wilson, K. M., Plane, J. M. C., and Penkett, S. A.: Intercomparison of formaldehyde measurements in clean and polluted atmospheres, J. Atmos. Chem., 37, 53–80, 2000. 6986, 7016

Christian, H., Blakslee, R., Boccippio, D., Boek, W., Buechler, D., Driscoll, K., Goodman, S., Hall, J., Koshak, W., Mach, D., and Stewart, M.: Global frequency and distribution of lightning as observed by the Optical Transient Detector, J. Geophys. Res., 108, doi:10.1029/2002JD002347, 2003. 6983

Crassier, V., Shure, K., Tulet, P., and Rosset, R.: Development of a reduced chemical scheme for use in mesoscale meteorological models, Atmos. Environ., 34, 2633–2644, 2000. 6987, 7017

Cros, B., Fontan, J., Minga, A., Helas, G., Nganga, D., Delmas, R., Chapuis, A., Benech, B., Druilhet, A., and Andrea, M.: Vertical profiles of ozone between 0 and 400 m in and above an African Equatorial forest, J. Geophys. Res., 97, 12877–12877, 1992. 6984

Cros, B., Delon, C., Affre, C., Marion, T., Druilhet, A., Perros, P., and Lopez, A.: Sources and sinks of ozone in savanna forest areas during EXPRESSO: Airborne turbulent flux measurements, J. Geophys. Res., 105, 29347–29358, 2000. 6984

Cuxart, J., Bougeault, P., and Redelsperger, J.-L.: A turbulence scheme allowing for mesoscale and large-eddy simulations, Q. J. Roy. Meteor. Soc., 126, 1–30, 2000. 6986

DeCaria, A., Pickering, K., Stenchikov, G., and Ott, L.: Lightning-generated NO_x and its impact on tropospheric ozone production: A three dimensional modeling study of a Stratosphere-Troposphere Experiment: Radiation, Aerosols and Ozone (STERAO-A) thunderstom, J. Geophys. Res., 110, doi:10.1029/2004JD005556, 2005. 6983

Delon, C., Reeves, C. E., Stewart, D. J., Serça, D., Dupont, R., Mari, C., Chaboureau, J.-P., and Tulet, P.: Biogenic nitrogen oxide emissions from soils – impact on NO_x and ozone over West Africa during AMMA (African Monsoon Multidisciplinary Experiment): modelling study, Atmos. Chem. Phys., 8, 2351–2363, 2008, http://www.atmos-chem-phys.net/8/2351/2008/. 6983, 6988, 7004, 7006

Doskey, P., Kotamarthi, V., Fukui, Y., Cook, D., Breitbeil, F., and Wesly, M.: Air-surface exchange of peroxyacetyl nitrate at grassland site, J. Geophys. Res., 109, doi:10.1029/2004JD004533, 2004. 7004

Fan, S.-M., Wofsy, S., Bakwin, P., Jacob, D., and Fitzjarrald, D.: Atmopshere-Biosphere Exchange of CO_2 and O_3 in the Central Amazon Forest, J. Geophys. Res., 95, 16851–16864, 1990. 6984

Fanou, L., Mobio, T., Creppy, E., Fayomi, B., Fustoni, S., Moller, P., Kyrtopoulos, S., Georgiades, P., Loft, S., Sanni, A., Skov, H., Ovrebo, S., and Autrup, H.: Survey of air pollution in Cotonou, Benin – air monitoring and biomarkers, Sci. Total Environ., 358, 85–96, doi:10.1016/j.scitotenv.2005.03.025, 2006. 6983

Gerbig, C., Schmitgen, S., Kley, D., Volz-Thomas, A., Dewey, K., and Haaks, D.: An improved fast-response vacuum UV resonance fluorescence CO instrument, J. Geophys. Res., 104, 1699–1704, 1999. 6985, 7016

Granier, C., Pétron, G., Müller, J.-F., and Brasseur, G.: The impact of natural and anthropogenic hydrocarbons on the tropospheric budget of carbon monoxide, Atmos. Environ., 34, 5255–5270, 2000. 7003

Granier, C., Lamarque, J. F., Mieville, A., Müller, J. F., Olivier, J., Orlando, J., Peters, J., Petron, G., and Tyndall, G.: POET, a database of surface emissions of ozone precursors, available on internet at http://www.aero.jussieu.fr/projet/ACCENT/POET.php, 2005. 6988, 6989

Gregory, G., Browell, E., and Warren, L.: Boundary-layer ozone – an airborne survey above the Amazon Basin, J. Geophys. Res., 93, 1452–1468, 1988. 6984

Guenther, A.and Hewitt, C. N., Erickson, D., Fall, R., Geron, C., Graedel, T., Harley, P., Klinger,

L., Lerdau, M., McKay, W. A., Pierce, T., Scholes, B., Steinbrecher, R., Tallamraju, R., Taylor, J., and Zimmerman, P.: A global model of natural volatile organic compound emissions, J. Geophys. Res., 100, 8873–8892, 1995. 6982

Hopkins, J. R., Evans, M. J., Lee, J. D., Lewis, A. C., Marsham, J. H., McQuaid, J. B., Parker, D. J., Stewart, D. J., Reeves, C. E., and Purvis, R. M.: Direct estimates of anthropogenic emissions from the megacity of Lagos, Atmos. Chem. Phys. Discuss., submitted, 2009. 6996

Jacob, D. J. and Wofsy, S. C.: Budgets of Reactive Nitrogen, Hydrocarbons and Ozone Over the Amazon Forest during the Wet Season, J. Geophys. Res., 95, 16737–16754, 1990. 6983, 6984, 6990, 6991, 6994, 7004

Jaeglé, L., Martin, R., Chance, K., Steinberger, L., Kurosu, T., Jacob, D., Modi, A., Yobou, V., Sigha-Nkamdjou, L., and Galy-Lacaux, C.: Satellite mapping of rain-induced nitric oxide emissions from soils, J. Geophys. Res., 109, doi:10.1020/2004JD004787, 2004. 6983, 6989, 7018

Jaeglé, L., Steinberger, L., Martin, R., and Chance, K.: Global partitionning of NO_x sources using satellite observations: relative roles of fossil fuel combustion, biomass burning and soils emissions, Faraday Discuss., 130, 1–17, 2005. 7004

Janicot, S., Thorncroft, C. D., Ali, A., Asencio, N., Berry, G., Bock, O., Bourles, B., Caniaux, G., Chauvin, F., Deme, A., Kergoat, L., Lafore, J.-P., Lavaysse, C., Lebel, T., Marticorena, B., Mounier, F., P., N., Redelsperger, J.-L., Ravegnani, F., Reeves, C. E., Roca, R., de Rosnay, P., Sultan, B., Tomasini, M., and Ulanovsky, A.: Large-scale overview of the summer monsoon over West during the AMMA field experiment in 2006, Ann. Geophys., 26, 2569–2595, 2008, http://www.ann-geophys.net/26/2569/2008/. 6993

Jonquière, I., Marenco, A., Maalej, A., and Rohrer, F.: Study of ozone formation and transatlantic transport from biomass burning emissions over West Africa during the airborne Tropospheric Ozone Campaigns TROPOZ I and TROPOZ II, J. Geophys. Res., 103, 19059–19073, 1998. 6982

Kesselmeier, J. and Staudt, M.: Biogenic organic volatile compounds (VOCs): An overview of emission, physiology and ecology, J. Atmos. Chem., 33, 23–88, 1999. 6982

Kirchhoff, V., Browell, E., and Gregory, G.: Ozone measurements in the troposphere of an Amazonian rain forest environment, J. Geophys. Res., 93, 15850–15860, 1988. 6984

Krol, M. C., Molemaker, M. J., and de Arellano, J. V. G.: Effects of turbulence and heterogeneous emissions on photochemically active species in the convective boundary layer, J. Geophys. Res., 105, 6871–6884, 2000. 6995

Labrador, L. J., von Kuhlmann, R., and Lawrence, M. G.: The effects of lightning-produced NO_x and its vertical distribution on atmospheric chemistry: sensitivity simulations with MATCH-MPIC, Atmos. Chem. Phys., 5, 1815–1834, 2005, http://www.atmos-chem-phys.net/5/1815/2005/. 6983

Lafore, J. P., Stein, J., Asencio, N., Bougeault, P., Ducrocq, V., Duron, J., Fischer, C., Héreil, P., Mascart, P., Masson, V., Pinty, J. P., Redelsperger, J. L., Richard, E., and Vilà-Guerau de Arellano, J.: The Meso-NH Atmospheric Simulation System. Part I: adiabatic formulation and control simulations, Ann. Geophys., 16, 90–109, 1998, http://www.ann-geophys.net/16/90/1998/. 6986

Lawrence, M., von Kuhlmann, R., and Salzmann, M.: The balance of effects of deep convective mixing on tropospheric ozone, Geophys. Res. Lett., 30, 1940, 2003. 6983

Lelieveld, J., Butler, T., Crowley, J. N., Dillon, T. J., Fisher, H., Ganzeveld, L., Harder, H., Lawrence, M. G., Martinez, M., Taraborrelli, D., and Williams, J.: Atmospheric oxidation capacity sustained by a tropical forest, Nature, 452, doi:10.1038/nature06870, 2008. 6994

Linden, J., Thorsson, S., and Eliasson, I.: Carbon Monoxide in Ouagadougou, Burkina Faso – A comparison between urban background, roadside and in-traffic measurements, Water Air Soil Pollut., 188, 345–353, doi:10.1007/s11270-007-9538-2, 2008. 6983

Mahfouf, J.-F. and Noilhan, J.: Inclusion of gravitational drainage in a land surface scheme based on the forced-restore method, J. Appl. Meteorol., 35, 987–992, 1996. 6987

Mari, C., Jacob, D., and Bechtold, P.: Transport and scavenging of soluble gases in deep convection cloud, J. Geophys. Res., 105, 22255–22267, 2000. 6986

Mari, C., Chaboureau, J. P., Pinty, J. P., Duron, J., Mascart, P., Cammas, J. P., Gheusi, F., Fehr, T., Schlager, H., Roiger, A., Lichtenstein, M., and Stock, P.: Regional lightning NO_x sources during the TROCCINOX experiment, Atmos. Chem. Phys., 6, 5559–5572, 2006, http://www.atmos-chem-phys.net/6/5559/2006/. 6987

Mari, C. H., Cailley, G., Corre, L., Saunois, M., Attié, J. L., Thouret, V., and Stohl, A.: Tracing biomass burning plumes from the Southern Hemisphere during the AMMA 2006 wet season experiment, Atmos. Chem. Phys., 8, 3951–3961, 2008, http://www.atmos-chem-phys.net/8/3951/2008/. 6982, 6992

Martin, R. V., Jacob, D. J., Logan, J. A., Ziemke, J. M., and Washington, R.: Detection of a lightning influence on tropical tropospheric ozone, Geophys. Res. Lett., 27(11), 1639–1642, 2000. 6983

Martin, R. V., Sauvage, B., Folkins, I., Sioris, C. E., Boone, C., Bernath, P., and Ziemke, J.:

Space-based constraints on the production of nitric oxide by lightning, J. Geophys. Res., 112, doi:10.1020/2006JD007831, 2007. 6983

Matsuda, K., Watanabe, I., Wingpud, V., Theramongkol, P., and Ohizimi, T.: Deposition velocity of O_3 and SO_2 in the dry and wet season above a tropical forest in northern Thailand, Atmos. Environ., 40, 7557–7564, 2006. 6984, 6989, 7019

Mondon, S. and Redelsperger, J.-L.: A study of a fair weather boundary layer in togacoare: parametrization of surface fluxes in large scale and regional models for light wind conditions, Bound.-Lay. Meteorol., 88, 47–76, 1998. 6987

Müller, J.-F., Stavrakou, T., Wallens, S., De Smedt, I., Van Roozendael, M., Potosnak, M. J., Rinne, J., Munger, B., Goldstein, A., and Guenther, A. B.: Global isoprene emissions estimated using MEGAN, ECMWF analyses and a detailed canopy environment model, Atmos. Chem. Phys., 8, 1329–1341, 2008, http://www.atmos-chem-phys.net/8/1329/2008/. 6988, 7018

Murphy, J., Oram, D., and Reeves, C.: PTr-MS measurements of isoprene, acetone, acetonitrile over West Africa, in preparation, Atmos. Chem. Phys. Discuss., 2009. 6984, 6985, 6992, 6998, 7007, 7016

Parker, D., Burton, R., Diongue-Niang, A., Ellis, R., Felton, M., Tayloy, C., Thorncroft, C., Bessemoulin, P., and Tompkins, A.: The diurnal cycle of the West African monsoon circulation, Q. J. Roy. Meteor. Soc., 131, 2839–2860, 2005. 6997

Peyrillé, P. and Lafore, J.-P.: An idealized two-dimensional framework to study the West African monsoon, part II: large scale advection and the diurnal cycle, J. Atmos. Sci., 64, 2783–2803, 2007. 6997

Peyrillé, P., Lafore, J.-P., and Redelsperger, J.-L.: An idealized two-dimensional framework to study the West African monsoon, part I: Validation and key controlling factors, J. Atmos. Sci., 64, 2765–2782, 2007. 6984, 6986, 6987

Pfister, G., Emmons, L., Hess, P. G., Lamarque, J.-F., Orlando, J., Walters, S., Guenther, A., Palmer, P., and Lawrence, P.: Contribution of isoprene to chemical budgets: A model tracer study with the NCAR CTM MOZART-4, J. Geophys. Res., 113, doi:10.1029/2007JD008948, 2008. 6982, 7002, 7003

Pickering, K. E., Thompson, A. M., Wang, Y., Tao, W.-K., McNamara, D. P., Kirchhoff, V. M. J. H., Heikes, B. G., Sachse, G. W., Bradshaw, J. D., Gregory, G. L., and Blake, D. R.: Convective transport of biomass burning emissions over Brazil during TRACE A, J. Geophys. Res., 101, 23993–24012, 1996. 6983

Price, C. and Rind, D.: A simple lightning parametrization for calculating global lightning distributions, J. Geophys. Res., 97, 9919–9933, 1992. 6987

Price, C. and Rind, D.: What determines the cloud-to-ground lightning fraction in thunderstorm?, J. Geophys. Res., 20, 463–466, 1993. 6987

Reeves, C., Ancellet, G., Borgon, A., Cairo, F., Mari, C., Methven, J., Schlager, H., and Thouret, V.: Chemical characterisation of the West Africa monsoon during AMMA, in preparation, Atmos. Chem. Phys. Discuss., 2009. 6982, 6984, 6985, 6992, 6993

Reynolds, R. and Smith, W.: A high-resolution global sea surface temperatures climatology, J. Climate, 8, 1571–1583, 1995. 6986

Rummel, U., Ammann, C., Kirkman, G. A., Moura, M. A. L., Foken, T., Andreae, M. O., and Meixner, F. X.: Seasonal variation of ozone deposition to a tropical rain forest in southwest Amazonia, Atmos. Chem. Phys., 7, 5415–5435, 2007, http://www.atmos-chem-phys.net/7/5415/2007/. 6984, 6989

Saunois, M., Mari, C., Thouret, V., Cammas, J., Peyrillé, P., Lafore, J., Sauvage, B., Volz-Thomas, A., Nédélec, P., and Pinty, J.: An idealized two-dimensional approach to study the impact of the West African monsoon on the meridional gradient of tropospheric ozone, J. Geophys. Res., 113, doi:10.1029/2007JD008707, 2008. 6983, 6984, 6986, 6988, 7001

Sauvage, B., Thouret, V., Cammas, J.-P., Gheusi, F., Athier, G., J., and Nédélec, P.: Tropospheric ozone over Equatorial Africa : regional aspects from the MOZAIC data, Atmos. Chem. Phys., 5, 311–335, 2005, http://www.atmos-chem-phys.net/5/311/2005/. 6982

Sauvage, B., Martin, R. V., van Donkelaar, A., Liu, X., Chance, K., Jaeglé, L., Palmer, P. I., Wu, S., and Fu, T.-M.: Remote sensed and in situ constraints on processes affecting tropical tropospheric ozone, Atmos. Chem. Phys., 7, 815–838, 2007a, http://www.atmos-chem-phys.net/7/815/2007/. 6992

Sauvage, B., Martin, R. V., van Donkelaar, A., and Ziemke, J. R.: Quantification of the factors controlling tropical tropospheric ozone and the South Atlantic maximum, J. Geophys. Res., 112, doi:10.1029/2006JD008008, 2007b. 6982, 6983

Sauvage, B., Thouret, V., Cammas, J.-P., Brioude, J., Nédélec, P., and Mari, C.: Meridional ozone gradients in the African upper troposphere, Geophys. Res. Lett., 34, doi:10.1029/2006GL028542, 2007c. 6983

Schultz, M., Pulles, T., Brand, R., van het Bolscher, M., and Dalsøren, S.: A global data set of anthropogenic CO, NO_x, and NMVOC emissions for 1960–2000, in preparation, 2005. 6989, 7018

Seinfeld, J. and Pandis, S.: Atmospheric Chemistry and Physics: From Air Pollution to Climate Change, John Wiley & Sons, 19, 958–960, 1998. 6989, 7019

Shindell, D. T., Faluvegi, G., Stevenson, D. S., Krol, M. C., Emmons, L. K., Lamarque, J.-F., Pétron, G., Dentener, F. J., Ellingsen, K., Schultz, M. G., Wild, O., Amann, M., Atherton, C. S., Bergmann, D. J., Bey, I., Butler, T., Cofala, J., Collins, W. J., Derwent, R. G., Doherty, R. M., Drevet, J., Eskes, H. J., Fiore, A. M., Gauss, M., Hauglustaine, D. A., Horowitz, L. W., Isaksen, I. S. A., Lawrence, M. G., Montanaro, V., Müller, J.-F., Pitari, G., Prather, M. J., Pyle, J. A., Rast, S., Rodriguez, J. M., Sanderson, M. G., Savage, N. H., Strahan, S. E., Sudo, K., Szopa, S., Unger, N., van Noije, T. P. C., and Zeng, G.: Multimodel simulations of carbon monoxide: Comparison with observations and projected near-future changes, J. Geophys. Res., 111, D19306, doi:10.1029/2006JD007100, 2006. 6991

Singh, H., Herlth, D., O'Hara, D., Salas, L., Torres, A., Gregory, G., Sachse, G., and Kasting, J.: Atmospheric Peroxyacetyl Nitrate Measurements Over the Brazilian Amazon Basin During the Wet Season: Relationships With Nitrogen Oxides and Ozone, J. Geophys. Res., 95, 16945–16954, 1990. 7004

Stewart, D. J., Taylor, C. M., Reeves, C. E., and McQuaid, J. B.: Biogenic nitrogen oxide emissions from soils: impact on NO_x and ozone over west Africa during AMMA (African Monsoon Multidisciplinary Analysis): observational study, Atmos. Chem. Phys., 8, 2285–2297, 2008, http://www.atmos-chem-phys.net/8/2285/2008/. 6982, 6983, 6988, 6995, 6996, 7004, 7006

Stickler, A., Fischer, H., Bozem, H., Gurk, C., Schiller, C., Martinez-Harder, M., Kubistin, D., Harder, H., Williams, J., Eerdekens, G., Yassaa, N., Ganzeveld, L., Sander, R., and Lelieveld, J.: Chemistry, transport and dry deposition of trace gases in the boundary layer over the tropical Atlantic Ocean and the Guyanas during the GABRIEL field campaign, Atmos. Chem. Phys., 7, 3933–3956, 2007, http://www.atmos-chem-phys.net/7/3933/2007/. 6999

Stockwell, W., Kirchner, F., Kuhn, M., and Seefeld, S.: A new mechanism for regional atmospheric chemistry modeling, J. Geophys. Res., 102, 25847–25879, 1997. 6987, 6991

Sumner, A. L., Shepson, P., Couch, T., Thornberry, T., Carroll, M. A., Sillman, S., Pippin, M., Bertman, S., Tan, D., Faloona, I., Brune, W., Young, V., Cooper, O., Moody, J., and Stockwell, W.: A study of formaldehyde chemistry above forest canopy, J. Geophys. Res., 106, 24387–24405, 2001. 7000

Thompson, A. M.: The oxidizing capacity of the Earth's atmosphere: probable past and future changes, Science, 256, 1157–1165, 1992. 6982

Thouret, V., Saunois, M., Minga, A., Brioude, J., Sauvage, B., Mariscal, A., Solete, A., Agbangla, D., and Nédélec, P.: Two years of Ozone radio soundings over Cotonou in the frame of AMMA: Overview, in preparation, Atmos. Chem. Phys. Discuss., 2009. 6982

von Kuhlmann, R., Lawrence, M., Crutzen, P., and Rasch, P.: A model for studies of tropospheric ozone and non-methane hydrocarbons: Model description and ozone results, J. Geophys. Res., 108, doi:10.1029/2002JD002893, 2003. 6989, 7019

Wang, G. and Eltahir, E.: Biosphere-atmosphere interactions over West Africa. II: Multiple climate equilibria, Q. J. Roy. Meteor. Soc., 126, 1261–1280, 2000. 6982, 7003

Table 1. Synopsis of the measurements on the FAAM BAe-146 Atmospheric Research Aircraft during AMMA.

Species/Parameters	Reference	Technique	Averaging time	Accuracy	Precision	Detection limit
O_3		UV	3 s	5%	1 ppbv	2 ppbv
CO	Gerbig et al. (1999)	VUV fluorescence	1 s		1 ppbv	2 ppbv
Oxygenates	Murphy et al. (2009)	PTR-MS	1–2 s	10–50%	10%	20–80 pptv
NO_x		TECO	1 s	50 ppt	–	50 ppt
CH_2O	Cardenas et al. (2000)	Fluorometric	10 s	30%	12%	50 pptv

ACPD
9, 6979–7032, 2009

Table 2. Description of some of the species modelled in ReLACs chemical mechanism. See Crassier et al. (2000) for further details.

ReLACS species	Brief description
ETH	ethane
ALKA	alkanes, alkynes, alcohols, esters...
ALKE	ethene and higher alkene
BIO	isoprene + α-pinene + d-limonene ...
HCHO	formaldehyde
ALD	acetaldehyde and higher saturated aldehydes
KET	acetone and higher saturated ketones
CARBO	other carbonyls (among them: methacrolein..)
ARO	aromatic species
PAN	PAN, higher and unsaturated PANs
OP1	methyl hydrogen peroxide CH_3OOH
OP2	higher organic peroxides
BIOP	peroxy radicals formed from BIO
MO2	Methyl peroxy radical
ETHP	peroxy radicals formed from ETH
ALKAP	peroxy radical formed from ALKA
ALKEP	peroxy radical formed from ALKE
BIOP	peroxy radical formed from BIO
CARBOP	acetyl peroxy radicals (+ higher saturated and unsaturated) and peroxy radicals formed from KET

ACPD
9, 6979–7032, 2009

Table 3. Surface emission fluxes in molecules cm^{-2} s^{-1} assigned in the model. Natural emissions from ocean and vegetation are adapted from the POET/GEIA inventory except for isoprene and terpenes that are derived from Müller et al. (2008) and for NO_x emissions that are adapted from both POET/GEIA and Jaeglé et al. (2004). The anthropogenic emissions are adapted from the RETRO 2000 inventory (Schultz et al., 2005). Model species names are capitalized. Numbers in parentheses correspond to aggregation factors used to combine real species. See text for details.

Source	Ocean	Vegetation	Soils		Anthropogenic	
Location	<5° N & >30° N	5° N–12° N	5° N–12° N	12° N–16° N	5° N–8° N	8° N–14° N
CO	0.29E10	0.17E12	0	0	0.51E12	0.11E12
NO_x	0	0	0.17E11	0.45E11	0.12E11	0.25E10
BIO						
isoprene (1)	0	0.22E12	0	0	0	0
terpenes (1)	0	0.22E11	0	0	0	0
ETH	0.13E9	0.99E9	0	0	0.39E10	0.94E9
ALKA						
propane (0.44)	0.12E9	0.13E10	0	0	0.13E10	0.34E9
butane (0.85)	0	0	0	0	0.20E10	0.54E9
higher alkanes (1.20)	0	0	0	0	0.37E10	0.60E9
methanol (0.38)	0	0.75E11	0	0	0	0
alcohols RETRO (lumped)	0	0	0	0	0.75E10	0.18E10
ethyne (0.31)	0	0	0	0	0.30E10	0.70E9
ALKE						
ethene (0.96)	0.20E9	0.53E10	0	0	0.72E10	0.17E10
propene (1.04)	0.15E9	0.71E9	0	0	0.21E10	0.51E9
KET						
acetone (0.33)	0	0.15E9	0	0	0.11E10	0.28E9
HCHO	0	0	0	0	0.12E10	0.28E9
ALD	0	0	0	0	0.22E10	0.52E9

ACPD
9, 6979–7032, 2009

Table 4. Dry deposition velocities in $cm\,s^{-1}$ adopted from Seinfeld and Pandis (1998) for NO, NO_2, HNO_3, H_2O_2 and from von Kuhlmann et al. (2003) for HCHO, aldehydes, PAN. O_3 deposition velocities are taken from Seinfeld and Pandis (1998) over ocean and desert and from Matsuda et al. (2006) over vegetation.

	Ocean	Vegetation	Desert+Bare soil
O_3	0.07	0.65	0.1
NO	0.003	0.016	0.003
NO_2	0.02	0.1	0.02
H_2O_2	1.0	0.5	1.0
HNO_3	1.0	4.0	1.0
HCHO	0.9	0.36	0.36
OP1	0.35	0.18	0.18
PAN	0.02	0.1	0.1

ACPD
9, 6979–7032, 2009

Table 5. Relative contributions of chemistry, convection, turbulence and advection to the ozone budget during daytime, nighttime as well as 24 h averages for the three regions described in the text.

	5° N–12° N			12° N–16° N			16° N–20° N		
	day	night	24 h	day	night	24 h	day	night	24 h
chemistry	0.58	−0.07	0.26	1.37	−0.12	0.63	0.32	−0.02	0.15
convection	0.14	0.15	0.14	0.02	0.05	0.04	0.08	−0.005	0.04
turbulence (deposition)	−0.41	−0.34	−0.37	−0.16	−0.13	−0.15	−0.30	−0.14	−0.22
horiz. adv.	−0.28	−0.05	−0.16	0.19	0.10	0.15	0.76	0.56	0.67
vert.adv.	0.27	0.03	0.15	−0.59	−0.57	−0.58	−0.73	−0.49	−0.61
total adv.	−0.005	−0.012	−0.01	−0.39	−0.48	−0.43	−0.02	0.07	0.05
total tend.	0.30	−0.27	0.02	0.84	−0.68	0.08	0.14	−0.10	0.02

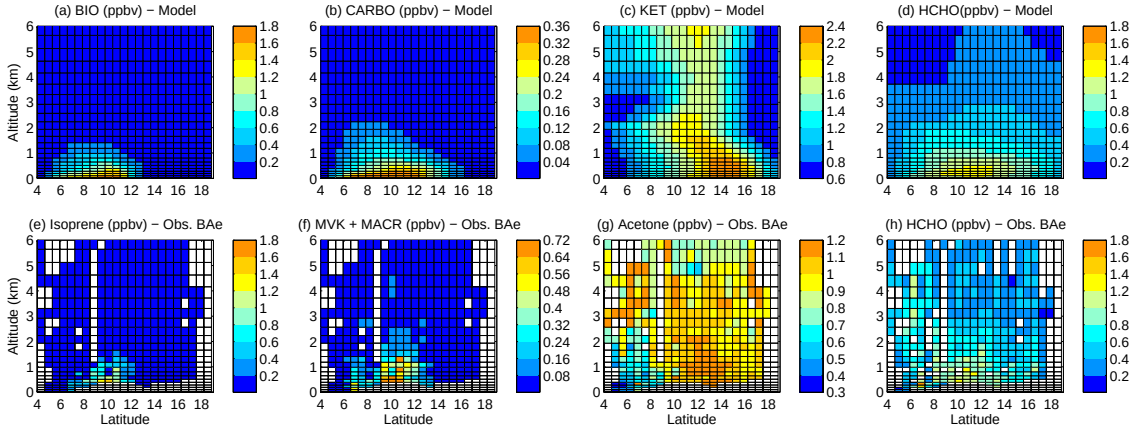

Fig. 1. Meridional vertical cross sections of the simulated BIO, CARBO, KET and HCHO (top) and of the observed (bottom) isoprene, MVK+MACR, acetone and HCHO averaged in the model bin in ppbv between 4° N and 19° N from the surface up to 6 km.

ACPD
9, 6979–7032, 2009

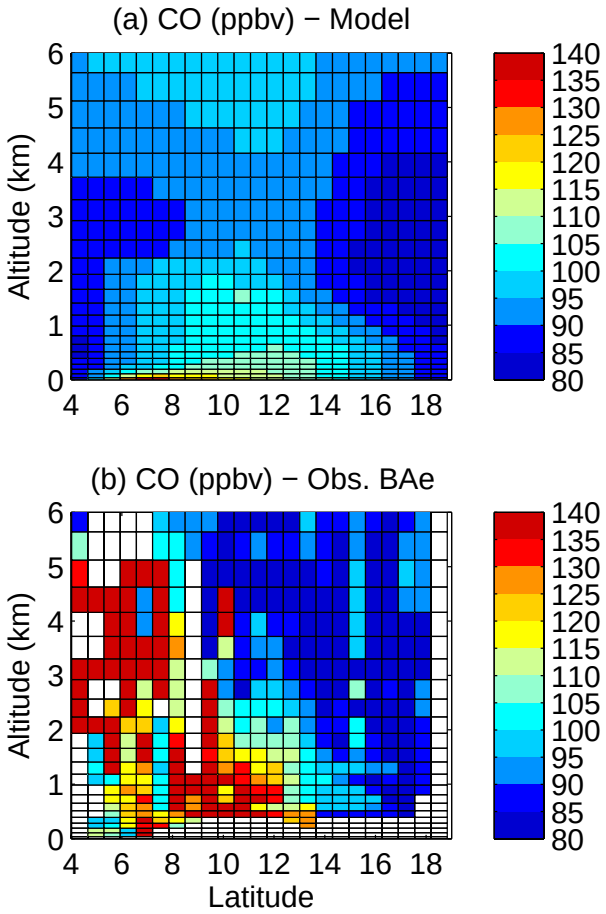

Fig. 2. Meridional vertical cross sections of the simulated **(a)** and observed **(b)** CO in ppbv between 4° N and 19° N from the surface up to 6 km.

ACPD
9, 6979–7032, 2009

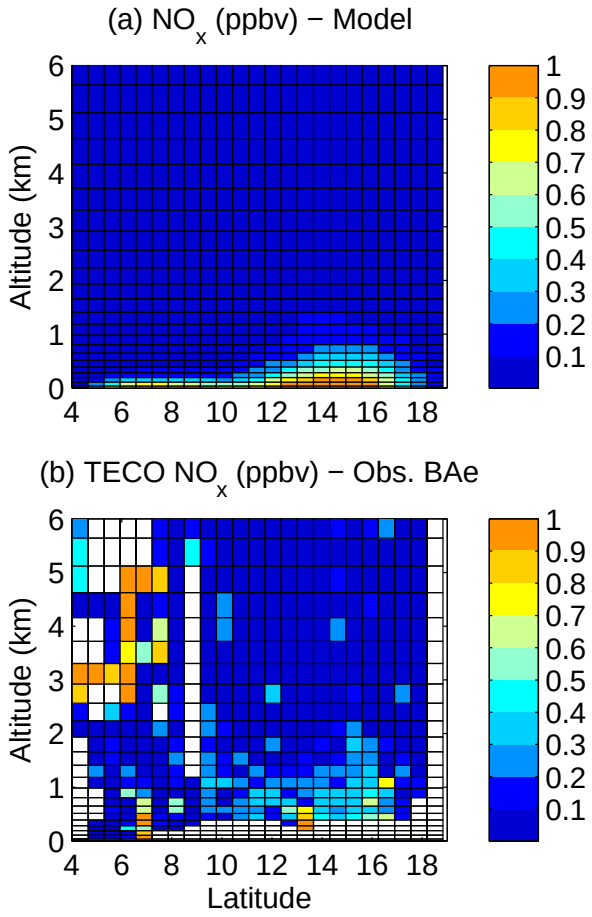

Fig. 3. Meridional vertical cross sections of the simulated **(a)** and observed **(b)** NO_x in ppbv between 4° N and 19° N from the surface up to 6 km.

ACPD
9, 6979–7032, 2009

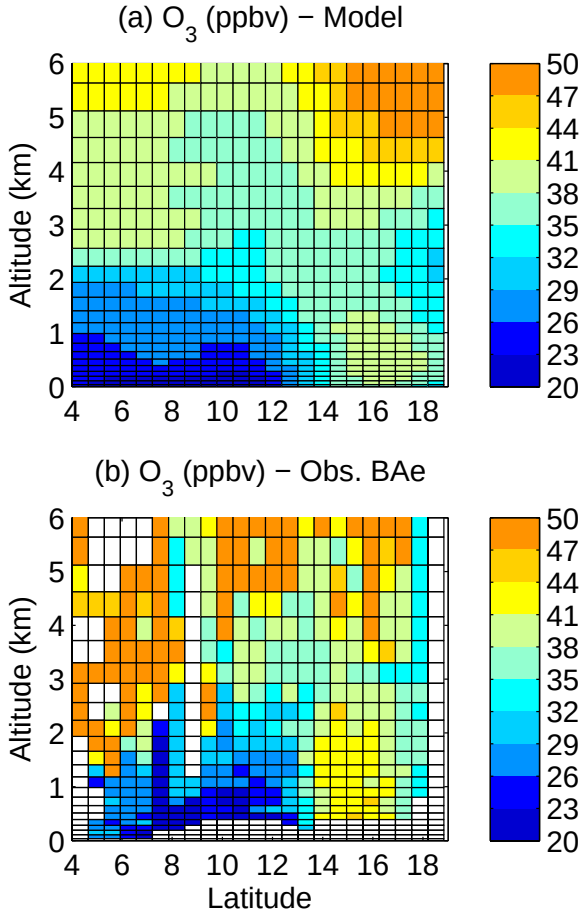

Fig. 4. Meridional vertical cross sections of the simulated **(a)** and **(b)** observed O_3 in ppbv between 4° N and 19° N from the surface up to 6 km.

ACPD
9, 6979–7032, 2009

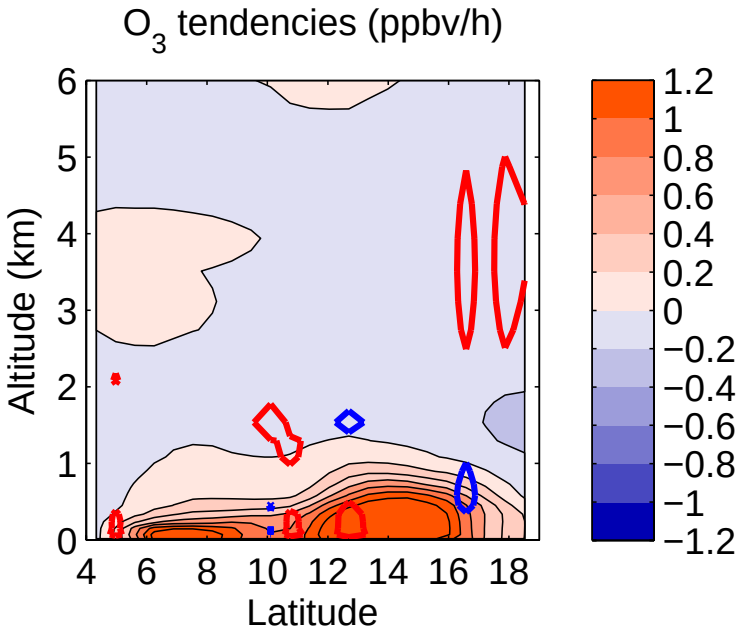

Fig. 5. Meridional vertical cross section of the simulated O_3 chemical (coloured area) tendency during daytime in ppbv h^{-1} between 4° N and 19° N from the surface up to 6 km. Isolines for convective tendencies at −0.5 ppbv h^{-1} (blue) and +0.5 ppbv h^{-1} (red) are over plotted.

ACPD
9, 6979–7032, 2009

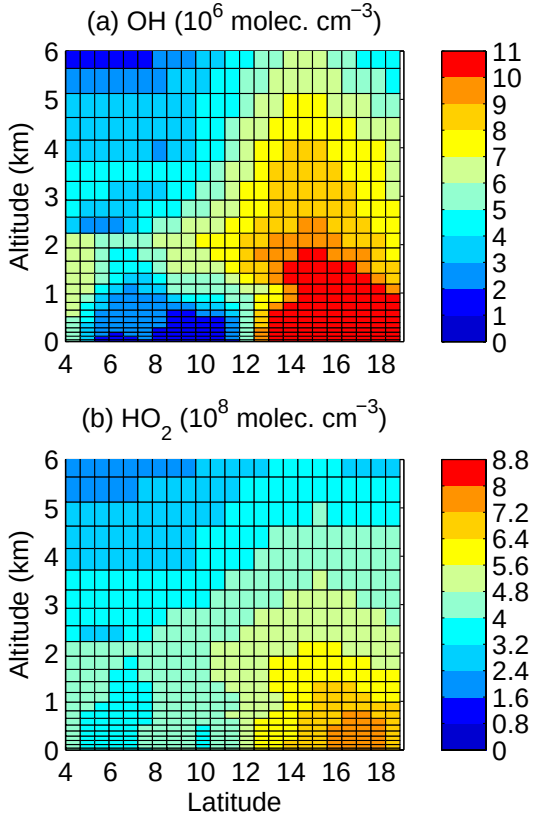

Fig. 6. Meridional vertical cross sections of OH (top) in 10^6 molec cm^{-3} and HO_2 (bottom) in 10^8 molec cm^{-3} between 4° N and 19° N from the surface up to 6 km simulated at 12:00 UTC the 26th day.

ACPD
9, 6979–7032, 2009

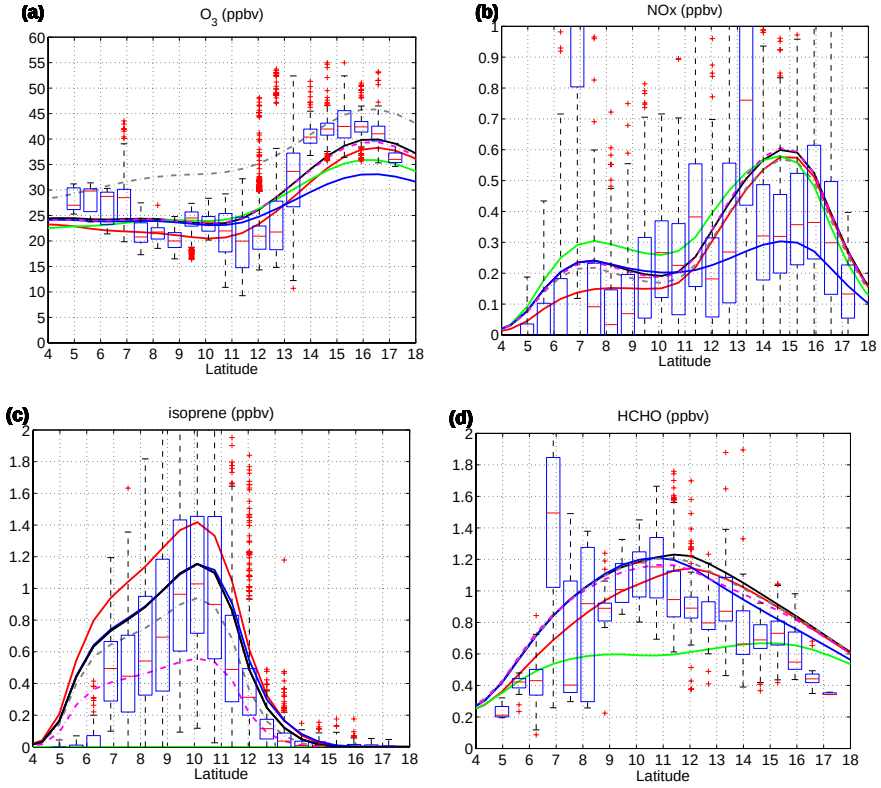

Fig. 7. 24 h-averaged modelled meridional profiles of O_3, BIO, CARBO, CO, NO_x, KET, HCHO in ppbv in the layer 0–700 m. For the reference run (RETRO) and sensitivity runs for BIO emissions (NOISO), anthropogenic emissions (NOANT), ozone dry deposition (NODEP) NO_x emissions from soils (IDSOL) and artificial OH recycling OHRE2. The box-plot shows the measurements average in the grid point and below 700 m. The median is in red and the first and third quartile are in blue. The extent of the data is represented by the whisker (limit at 0.5 time the interquartile range) and the red crosses.

ACPD
9, 6979–7032, 2009

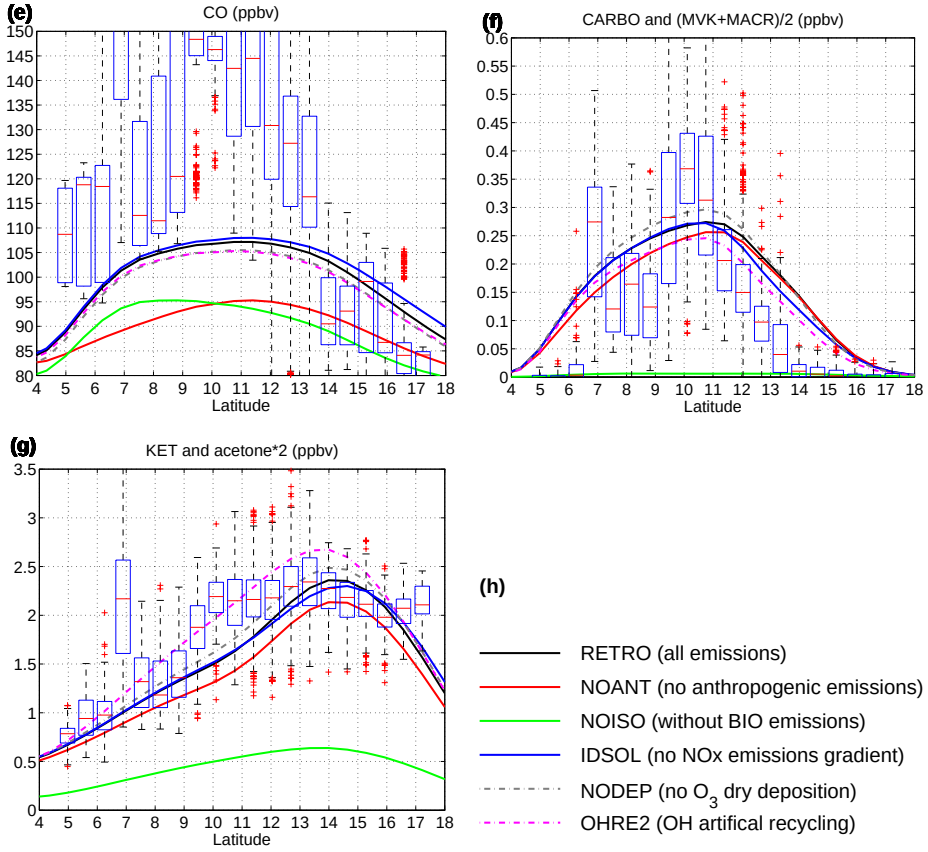

Fig. 7. Continued.

ACPD
9, 6979–7032, 2009

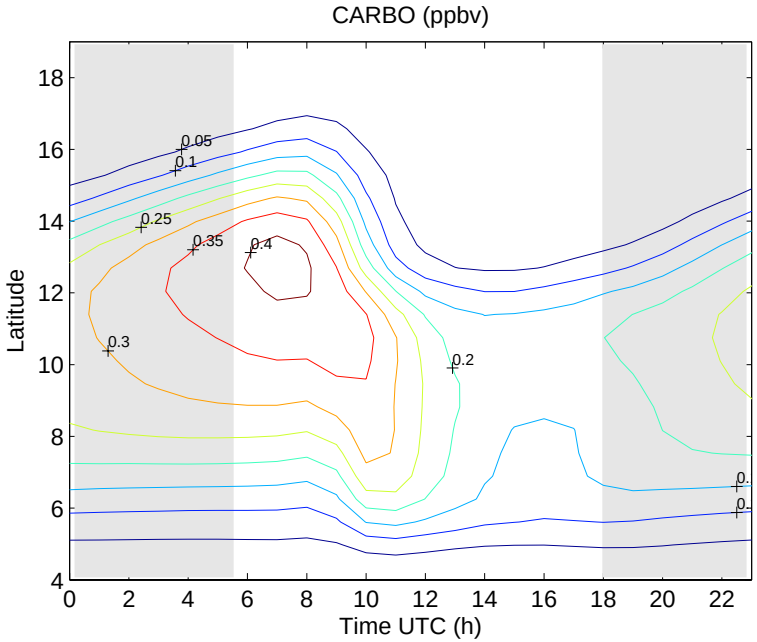

Fig. 8. Composite diurnal cycle of the simulated CARBO mixing ratios below 700 m in ppbv between 4° N and 19° N for the reference run. Night time is shaded in grey.

ACPD
9, 6979–7032, 2009

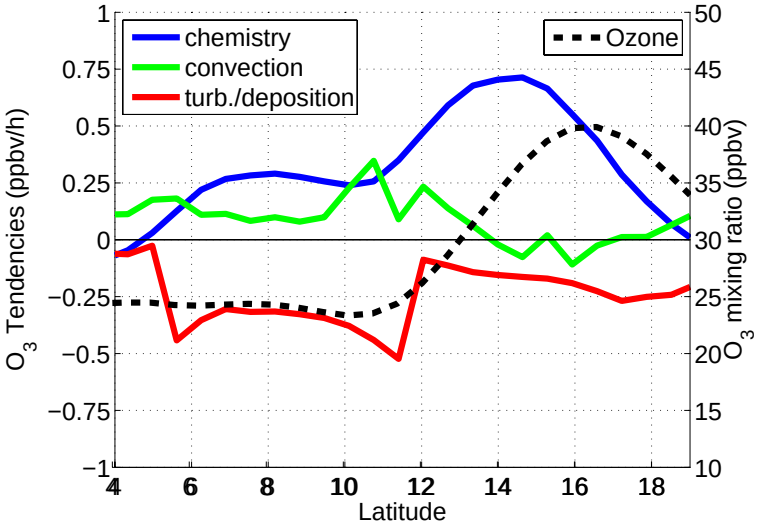

Fig. 9. 24h-average meridional profiles of O_3 and its chemical, convective and turbulent tendencies in the layer 0–700 m in ppbv or ppbv/h between 4° N and 19° N for the reference run.

ACPD
9, 6979–7032, 2009

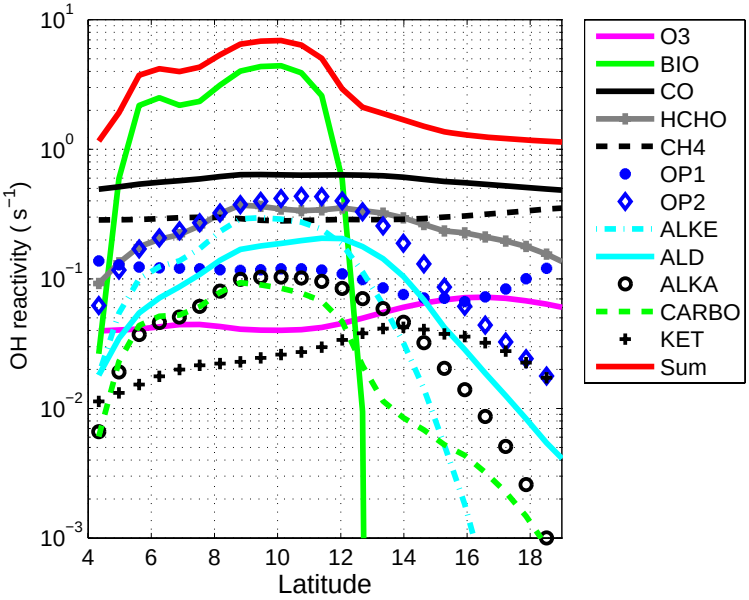

Fig. 10. OH reactivity for species that contribute to more than 0.1% of the total at 12:00 UTC below 700 m between 4° N and 19° N for the reference run in s^{-1}.

ACPD
9, 6979–7032, 2009

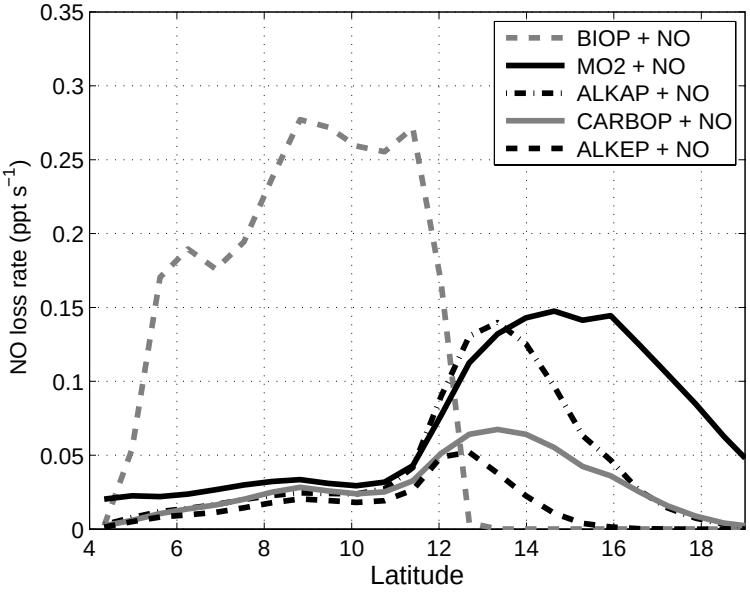

Fig. 11. Mean NO loss rates for its reaction with the peroxy radicals: BIOP, CARBOP, ALKAP, ALKEP and MO2 at 12:00 UTC below 700 m between 4° N and 19° N for the reference run in ppt s^{-1}.

ACPD
9, 6979–7032, 2009